Open access • Posted Content • DOI:10.1101/743294

Wheat inositol pyrophosphate kinase (TaVIH2-3B) interacts with Fasciclin-like arabinogalactan (FLA6) protein and alters the plant cell-wall composition

Mandeep Kaur, Anuj Shukla, Swati Kanwar, Vishnu Shukla ...+9 more authors

Institutions: Department of Biotechnology, Indian Institute of Science

Published on: 27 Aug 2019 - bioRxiv (Cold Spring Harbor Laboratory)

Topics: Arabinogalactan protein, Arabinogalactan, Arabidopsis, Inositol and Complementation

Inositol pyrophosphate kinase (VIH2) impart drought resistance by promoting plant cell wall homeostasis

Author names and affiliations: Anuj Shukla[1], Mandeep Kaur[1,2], Swati Kanwar[1], Gazaldeep Kaur[1], Shivani Sharma[1], Koushik Mazumder[1], Pratima Pandey[3], Vikas Rishi[1] and Ajay K Pandey[1,*]

[1]National Agri-Food Biotechnology Institute (Department of Biotechnology), Sector 81, Knowledge City, S.A.S. Nagar, Mohali-140306, Punjab, India.

[2]Department of Biotechnology, Panjab University, Punjab, India.

[3]Department of Biological Sciences, Indian Institute of Education and Research, Mohali 140306.

**Corresponding author:*

Dr. Ajay K Pandey, Scientist-E

Email: pandeyak@nabi.res.in; pandeyak1974@gmail.com

ORCID iD: https://orcid.org/0000-0003-1064-139X

Abstract

Inositol pyrophosphates (PPx-InsPs) are important signalling molecules, those participate in multiple physiological processes across wide range of species. However, limited knowledge is available for their role in plants. Here, we characterized two diphosphoinositol pentakisphosphate kinase (PPIP5K) wheat homologs, *TaVIH1* and *TaVIH2* for their spatio-temporal expression and physiological functions. We demonstrated the presence of functional VIH-kinase domains through biochemical assays where high energy pyrophosphate forms ($IP_{7/8}$) were generated. Our GUS-reporter assays in *Arabidopsis*, suggested the role of *TaVIH2* in drought stress. Yeast two-hybrid screen of TaVIH2 by utilizing wheat library yielded multiple cell-wall related interacting partners. *TaVIH2* overexpression in Arabidopsis provided growth advantage and drought tolerance. Further, transcriptomic studies of these overexpressing lines showed activation of genes encoding for abscisic acid metabolism, cell-wall biosynthesis and drought responsive element binding proteins. Biochemical analysis of their cell-wall components, confirmed enhanced accumulation of polysaccharides (arabinogalactan, cellulose and arabinoxylan) in transgenics. These results reveal novel function of VIH proteins in modulating cell wall homeostasis thereby providing drought tolerance.

Keywords: Inositol pyrophosphate kinase, wheat, drought stress, phytic acid, transcriptome, cell wall

Introduction

Inositol pyrophosphates (InsPPs) are an important member of the inositol phosphate family that have emerged as distinct molecules possessing array of phosphates around an inositol ring [1]. The role of high energy InsPPs including $InsP_7$ and $InsP_8$ has been studied in human cell lines and yeast. They were shown to participate in DNA recombination, vacuolar morphology, cell wall integrity, gene expression, pseudohyphal growth and phosphate homeostasis [2–7]. These InsPPs are predominantly synthesized by two different classes of enzymes that exhibit catalytic activity towards different positions on the six-C inositol ring. The first class of enzymes, Inositol hexakisphosphate kinases (IP_6Ks) place a phosphate group at 5th position of the fully phosphorylated ring of $InsP_6$/IP_6 to form 5PP-IP_5 ie IP_7 [8,9] and also generates two isomers of IP_8 including; 1or 3,5PP-IP_5 and 5PPP-IP_5 [10]. The second class of enzymes referred as diphosphoinositol pentakisphosphate kinases (PP-IP5Ks) phosphorylate the 1st position of IP_6 synthesizing 1PP-IP_5 [11–13]. These enzymes also catalyse the conversion of 5PP-IP_5 to 1,5$(PP)_2IP_4$ i.e. IP_8 which was first demonstrated in mammalian cells [1]. During the past two decades three isoforms of IP_6K (IP_6K1, IP_6K2 and IP_6K3) and two PP-IP5K (PP-IP5K1 and PP-IP5K2) were identified in mammals [1]. In yeast, a single IP_6K (also referred as Kcs1) and PP-IP5K (also known as VIP1/IP_7K) are present that are involved in synthesis of the respective forms of IP_7 and IP_8 [12,13]. VIPs are also referred as VIH in plants and are dual domain containing proteins; including a “rim-K” or ATP-grasp superfamily domain at the N-terminal and a C-terminal histidine acid-phosphatase domain [13].

In plant seeds, the most abundant inositol polyphosphate referred as, Inositol hexa*kis*phosphate (Phytic acid,IP_6) is the primary source of stored phosphorus (P) which is utilized by the plants to draw energy during the process of seed germination. Earlier, the presence of high anionic form of IP_6 was speculated in plant species such as barley and potato [14,15]. The quest to identify the plant genes encoding for these inositol pyrophosphate kinases remained elusive till the identification of two plant genes referred as VIP/VIH from *Arabidopsis* [16]. These VIH proteins were characterized to bear $PPIP_5K$ activity and shown to be involved in plant defense response that is mediated through jasmonate levels [16,17]. These identified VIH show functional activity in yeast mutants with their ability to rescue invasive growth with hyphae formation.

Recent evidence also implicates that IP_8 binds the SPX region of the SPX1 protein and control its interaction with a phosphate starvation response1, a central regulator of phosphate starvation [18]. Furthermore, in yeast, role of inositol pyrophosphate kinase was also implicated in vacuolar morphology and cell wall integrity [3]. Histone H3/H4 chaperone, Asf1p is known

to interact with the VIP1 (VIH) protein, thereby, suggesting this interaction important for transcription elongation [19]. Therefore, the function of the protein could also be studied in context to their interacting partners. Such comprehensive interaction studies for VIH protein is also missing in plants that could provide new insight into their functional roles.

In the current study, we identified two functionally active wheat VIH genes capable of utilizing IP_6 and IP_7 as substrates under In-vitro condition to generate higher InsPP. Promoter fused GUS-reporter assays during different stress condition revealed specific response of VIH2-3B promoter during drought condition. We also demonstrated that, at the protein level wheat VIH2-3B interact with Fasciclin-like arabinogalactan protein (FLA6) and other multiple cell-wall related proteins. Furthermore, we concluded that wheat homoeolog VIH2-3B could impart tolerance to drought in transgenic *Arabidopsis* by altering the composition of plant cell-wall and regulating distinct transcriptomic re-arrangements. Taken together, our study provides novel insight for the possible function of plant VIH protein in drought stress tolerance.

Results

Phylogeny and spatial-temporal expression characterization of VIH genes in wheat tissue

Our efforts to identify potential wheat VIH-like sequences resulted in the identification of six genes with three homoeolog for each, *TaVIH1* and *TaVIH2* those were mapped to chromosome 3 and 4 respectively. The Kyte-Doolittle hydropathy plots indicated that wheat VIH proteins were devoid of any transmembrane regions (Supplementary Figure S1A). The analysis clustered plant VIH homologs together with TaVIH proteins close to their *Brachypodium* counterparts in the monocot specific clade (Figure 1A). Amino acid sequence alignment of wheat VIH protein sequences suggested the presence of conserved dual domain architecture with two distinct domains consisting of amino-terminal rimK/ATP GRASP fold and a histidine acid-phosphatase (HAP) of PPIP5K/VIP1 family (Supplementary Figure 1B). Wheat VIH1 and VIH2 show 72% sequence identity at the protein level. Among the two wheat VIH proteins, TaVIH1 show high identity of 78% with AtVIH proteins whereas, TaVIH2 show 70.0 and 70.6 % identity to both AtVIH1 and AtVIH2 respectively.

Transcript accumulation of *TaVIH* genes showed similar expression profiles for both genes with highest expression in leaf tissue followed by flag leaf, root and with the least expression in stem (Figure 1B). The transcript accumulation of *TaVIH1* was 1.5-fold higher than *TaVIH2* in all the tissues investigated. These findings suggest that both VIH genes are

preferentially expressed in leaf. The highest expression of both VIH genes was observed at late stages of grain filling with high transcript accumulation at 28 DAA stage (Figure 1C). Interestingly, the pattern of gene expression remained same for both wheat VIH, wherein *TaVIH1* showed 3-fold higher expression in comparison to *TaVIH2* at all stages. The expression profile in different grain tissues revealed a high expression of *TaVIH* genes in the aleurone layer which is ~ 4-fold higher than in the endosperm. Similar levels of transcript accumulation in the remaining grain tissues *viz.* embryo, glumes, and rachis; suggesting a ubiquitous expression in these tissues (Figure 1C).

In general, expression levels of *TaVIH1* were more than *TaVIH2* during all stages of wheat development (Figure 1D). Overall, our expression analysis using ExpVIP [20] database showed high expression of *TaVIH1* transcripts from B and D genomes. *TaVIH2* did not show any significant expression in majority of tissues, however a weak expression was found in the spikes (Supplementary Figure S2A). Our analysis shows differential expression patterns of VIH during abiotic and biotic stresses suggesting their role in different development processes and stress response (Supplementary Figure S2B).

Wheat inositol pyrophosphate kinase demonstrate PPIP$_5$K activity

The homology modelled structure of VIH proteins, based on human PPIP5K2 (hPPIP$_5$K2; PDB ID:3T9C) predicted two antiparallel β-sheets to co-ordinate the nucleotide analog AMP-PNP (Supplementary Figure 3A). Likewise, human and *Arabidopsis* homologs, wheat VIH proteins also appear to use only arginine and lysine residues in the inositol phosphate binding pocket, except for a serine residue (Supplementary Figure 3B). Next, yeast complementation assay for wheat VIH genes was carried out using growth assay on SD-Ura plates supplemented with 0, 2.5 and 5 mM 6-azuracil. Both the yeast strains transformed with wheat VIH genes were confirmed for their protein expression by using Western analysis (Fig. The wild type strain BY4741 showed an unrestricted growth phenotype, whereas *vip1Δ* transformed with empty pYES2 vector showed growth sensitivity at 2.5 and 5mM concentrations (Supplementary Figure 3C). To our surprise, the mutant strain transformed with pYES2-TaVIH1 could not revive growth defect on selection plates whereas, the pYES2-TaVIH2-3B was able to rescue the growth phenotype of *vip1Δ* strain. Under stress condition unlike wild type yeast, *vip1Δ* mutant do not form pseudo-hyphae. The complemented *vip1Δ* strain with pYES2-TaVIH2-3B rescued this phenotype during stress (Supplementary Figure 3D). Overall, our data suggest that *TaVIH2* derived from the B genome is capable of complementing the growth defects of *vip1Δ* strain.

In-vitro kinase assay was performed with the pure wheat VIH-kinase (KD) proteins (Supplementary Figure S4) to check its activity. The relative luminescence units (RLU) were recorded for TaVIH1-KD and TaVIH2-KD while using IP_6 as a substrate (Figure 2A). Our assays show a very high increase in the RLU for both the proteins in the presence of IP_6. Interestingly, the wheat VIH2 show ~15-fold higher luminescence response, suggesting its high activity when compared to the VIH1 protein (Figure 3C). This kinase activity was diminished in VIH (D-VIH) post denaturation, and the activity was not significantly different when compared to either Enzyme control (Ec) or substrate control (IP_6) reactions.

To check the substrate utilizing ability of wheat VIH proteins, reactions were performed using IP_6 and IP_7 that phosphorylated inositol molecule species which were visualized on PAGE as reported earlier [21]. Our assays suggested that wheat VIH proteins could utilize IP_6 as a substrate to generate IP_7 (Figure 2B; left panel; lane 3, 4), as was also found in the case of ScVIP protein (Figure 2B; left panel; lane 1). Next, we tested if IP_7 (generated by ScVIP) could be utilized by wheat VIH proteins. We observed that both the wheat VIH proteins (TaVIH1 and TaVIH2) could utilize IP_7 to generate IP_8 (Figure 2B; right panel, lane 1, 3). Moreover, ScVIP was also able to utilize IP7 generated by TaVIH1 and TaVIH2 (Figure 2B; right panel, lane 2,4). These experiments conclude that TaVIH proteins are functionally active, capable of using both IP_6 and IP_7 as a substrate under In-vitro conditions and may possess $PPIP_5K$ like activity. To further confirm the nature of the phosphorylated inositol molecule during In-vitro reactions, MALDI-Tof- mass spectroscopy (MS) was performed. MS analysis indicated a major signal at m/z of 739.009 that correspond to the mass of IP_7 for all the generated species (Figure 2C; left panel). Similarly, the VIH1 generated IP_8 showed phosphorylated inositol molecule with m/z 820.1 and additional expected acetonitrile adduct at 860.9 (Figure 2C; right panel). Whereas VIH2 derived IP_8 showed m/z at 860.9 corresponding to the IP_8-acetonitrile adduct (Supplementary Figure S5). This confirms formation of the IP_7 and IP_8 as phosphorylated forms of inositol molecules. Overall, our analysis confirms the functionality of VIH proteins and their ability to generate both IP_7 and IP_8.

Expression of *35S:TaVIH2* transgenic *Arabidopsis* display robust growth

To characterize the biological functions of TaVIH2, cDNA was overexpressed in *Arabidopsis*. In total, seven transgenic lines were pre-selected based on TaVIH2 expression as shown by western analysis and four transgenic lines (#Line2, #Line 4, #Line 5 and #Line 6) were selected for further characterization (Figure 3B). We observed that, at the vegetative stage TaVIH2 transgenic *Arabidopsis* show robust growth. Plants (14 days old seedlings) showed enhanced

rosette area cover and increased number of leaves compared to controls (Col-0 and Col-0-Ev (empty vector)) respectively (Figure 3B, C and D). These transgenic *Arabidopsis* also show enhanced branching with an overall increase in the length of the main shoot axis and leaf size compared to controls (Figure 4A). Primary and secondary shoots numbers were also enhanced in the transgenic *Arabidopsis* (Figure 4B). In general, no significant differences during the flowering stage were observed, yet the increased number of (20-24) of secondary shoots were evident when compared to control plants (12-15 shoots). These data suggest that expression of TaVIH2 in *Arabidopsis* impacts the overall growth of the plant.

VIH2-3B imparts resistance to drought stress

To investigate the promoter activities of *TaVIH1* and *TaVIH2*, 5' flanking regions (~ 1.5 Kb) of these genes were cloned and the comparative analysis revealed the presence of various hormones and abiotic stress responsive cis elements (Supplementary Figure S6A). The presence of these elements suggested that wheat *VIH* could be regulated by stress. Interestingly, the promoter of *VIH* contains multiple drought/dehydration responsive domains, a P1BS motif (GNATATNC) and PHO4 binding sites in promoter regions of both *TaVIH* genes (Supplementary Figure S6A). This motivated us to perform a preliminary screening experiments using *TaVIH*-promoter fused to β-glucuronidase (GUS)-reporter gene (pVIH1/2:GUS) in *Arabidopsis* (Col-0). Significant increase in GUS reporter activity of *pVIH2:GUS* lines indicate the ability of this promoter to sense the given stress and drive GUS reporter expression. To our surprise, *TaVIH2* promoter responded strongly to dehydration, drought stress and Pi-starvation (Supplementary Figure S6B and Figure 5A). A strong GUS expression was also visualized along the mid-vein and leaf base of the seedlings subjected to Pi-stress. A weak expression of *VIH2* promoter was observed in the presence of ABA and GA_3. Control (Empty-vector-EV) seedlings showed no visible GUS-staining. Based on our reporter assays, we speculate that TaVIH2 participates during drought stress response that was further investigated.

To further test the effect of drought like conditions, seedlings were exposed to drought-like conditions using mannitol (125 mM) and glycerol (10 %)[21]. Our data indicate the retardation of root growth in control *Arabidopsis* suggesting that the plants were sensitive to the presence of these metabolites. In contrast, TaVIH2 overexpression in *Arabidopsis* was able to escape the detrimental root growth (Figure 5B). This observation was highly significant among the transgenic lines suggesting that TaVIH2 could contribute to drought stress (Figure

5C). Next, rate of water loss was studied to account for its possible role in withstanding drought stress. The rate of water loss was very significant in the control plants as compared to the transgenic (Figure 5D). The water loss percentage was lowest in the transgenic *Arabidopsis* (40-46%) when compared to control plants (16-18%) after 8 hrs of incubation (Figure 5D). To further, confirm its contribution towards drought tolerance, the transgenic *Arabidopsis* and control plants were subjected to 14 days of water withholding (drought). This caused a dramatic withering of both control and transgenic *Arabidopsis* plants. However, when the plants were re-watered, high survival rates of ~50-65 % was observed in the transgenic plants, whereas no or very low (3%) rates were observed in control (Figure 5E). This indicates that the transgenic *Arabidopsis* overexpressing TaVIH2, escapes the effect of drought and improves survival rate by imparting drought tolerance.

Wheat VIH2 interacts with Fasciclin-like arabinogalactan protein (FLA)

To investigate the mechanism of TaVIH2 proteins in stress tolerance, we used yeast two-hybrid (Y2H) cDNA screening for its interacting partners. Protein expression of bait (VIH2) in the yeast cells was confirmed by Western blot analysis (Supplementary Figure S7A). Two pooled wheat cDNA libraries were prepared that resulted in the identification of 89 putative yeast colonies with a mating efficiency of 3.8 % (Supplementary Figure S7B and C). Subsequent stringent screening (α-Gal) of the colonies lead to the identification of ~52 putative interactors (Supplementary Figure S7D). Upon sequencing of the ORFs, clones appearing more than twice were considered for further studies. Careful analysis lead to the shortlisting of eleven strong potential (3-6 clones) interactors with high occurrence of the clones those were related to proteins involved in cell-wall related function (Table 1). Amongst these interactions most of the genes encode for cell-wall related function, including Fasciclin-like arabinogalactan protein (FLA), glycosyl-transferases and glycine-rich structural proteins. The most frequently (six times) interacting clone was identified as FLA protein and its detailed analysis was done. To further confirm this interaction, full-length cloning of *TaFLA6* cDNA (1.2 kb) was performed and transformed (TaFLA6:AD+TaVIH2:BD) into yeast. Growth of yeast colonies on -His/-Leu/-Trp (Auerobasidin) media (Figure 6A) and the In-vivo pull-down assay with co-expressed VIH2 (cMYC-tagged) and FLA6 fusion protein (HA-tagged) in yeast confirmed the full-length interaction of these two proteins (Figure 6B).

The FLA proteins are known to respond for different stress conditions and are to be involved in plant growth and development [22,23]. These observations suggest that VIH2 and its

interacting partners may participate in similar pathway. Our localization studies in yeast suggest that FLA6 was present on the yeast plasma membrane (Figure 6C). Similarly, localization of VIH2 suggest their presence in the cytoplasm and the rim of the plasma membrane. Wheat FLA6 encodes a 367 aa protein containing FAS-like arabinogalactan protein with presence of typical trans-membrane domain (TMD) and glycophosphatidyl-inositol (GPI) domain [24,25]. The protein hydropathy plot identified a hydrophobic region near GPI region at the C-termini (Figure 6D). Transcript expression study of interacting partners (*TaFLA6, TaGT* and *TaXat1),* showed significant upregulation in the shoot tissue when subjected to drought stress (Supplementary Figure S8). Similar observation for *TaFLA6, TaGT* and *TaXat1* was also obtained through exVIP gene expression analysis (Supplementary Figure S8). Significant increase in transcript accumulation was observed during grain development and seed maturation (Supplementary Figure S8). These data indicated that *TaFLA6* and *TaGT/Xat* show transcriptional changes during desiccation, a prerequisite step in grain maturation. Important interacting clones, including *TaGT* and *TaXat* were also expressed in other tissue including developing roots and grains (Supplementary Figure S8). Taken together, our data suggest that wheat *VIH2* and *FLA6* are co-expressed under drought stress and they interact at the protein level.

Transcriptomes suggest that *VIH2-3B* stimulate genes related to drought stress

We next explored the reasoning for robust phenotype and resistance to drought in transgenic Arabidopsis. For this, transcriptomic changes in 25 days old seedlings of control and two transgenic plants (#Line4 and #Line6) were compared. PCA of normalized expression abundances revealed a high level of correlation among biological replicates (n=3) in each transgenic line. PCA also indicates distinct cluster for overexpressing transgenic lines and controls (Supplementary Figure S9A). Based on analysis involving respective three biological replicates, a total of 626 and 261 genes were significantly up- and down-regulated (-1>Log FC >1.0) in #Line4 while 797 and 273 genes were up- and downregulated in #Line6 transgenic Arabidopsis lines compared to control plants (Supplementary Table S3). Overall, 605 genes were commonly differentially altered in the two transgenic lines with respect to control plants (Col-0(Ev)).

Multiple genes were commonly up-regulated in transgenic *Arabidopsis* compared to control plants (Figure 7A and Supplementary Table S3). Interestingly, high number of genes are constitutively activated in the transgenic *Arabidopsis* belongs to the dehydration response element binding (DREB) protein including Integrase-type DNA-binding superfamily proteins

and glycine rich proteins. Upon analysis of the GO terms, the highest number of genes for "stress related" and "cell-wall related activities" were enriched in the biological process and cellular component categories (Figure 7B). Strikingly, multiple genes involved in cell-wall biosynthesis, modification and degradation were also up-regulated in the transgenic plants (Figure 8A). In addition to that, distinct cluster of genes involved in Abscisic acid (ABA) biosynthesis were also significantly up-regulated among the different lines of transgenic *Arabidopsis* (Figure 8B). Notably, genes encoding for 9-*cis*-epoxycarotenoid dioxygenase (*AtNCED6* and *AtNCED9*) involved in ABA biosynthesis were also up-regulated. Multiple DREB encoding genes and cytochrome P450 (CYPs) related family genes (*CYP71A23, CYP94B3, CYP71B12, CYP96A2, CYP702A1, CYP707A3, CYP82C2, CYP76G1, CYP705A4, CYP71B10, CYP706A2, CYP81D11*) were also differentially regulated in the transgenic *Arabidopsis* (Figure 8C and D) Overall, we conclude that distinct cluster of genes potentially involved in drought and ABA stress were significantly up-regulated in these transgenic plants.

VIH2 affects ABA levels and regulates plant cell-wall composition

Multiple genes related to ABA biosynthesis were differentially expressed in VIH2 overexpressing *Arabidopsis*. To verify if the de-novo gene expression response to the ABA related genes could be correlated with the In-vivo levels, ABA levels were quantified in the leaves. We observed that accumulation of ABA was significantly higher (~3-4 fold) in transgenic *Arabidopsis* when compared to the control plants (Figure 9A). This average increase of ABA in all the four transgenic lines was statistically significant ($p<0.05$, Student's t test). Our data confirmed the involvement of ABA in the drought tolerance of transgenic lines.

To further draw the commonality between the gene expression pattern in VIH2 overexpressing *Arabidopsis* and due to drought, we analysed previously reported RNAseq data SRA:SRP075287 (under drought stress) for overlap of de-regulated genes. In total, 295 and 309 genes were commonly regulated in #Line4 and #Line6 (Figure 9B). Most of listed genes those were commonly regulated belong to the category of hormone metabolism, signalling, stress response, development and cell wall related functions (Figure 9C). Multiple genes related to CYPs and glycosyl transferases were highly enriched in the dataset (Table S5). These extended analysis supports the notion that VIH2-3B could impart activation of genes pertaining to drought. Overall, our molecular analysis helped in identifying sub-set molecular of components in transgenic plants that could impart basal drought resistance.

Multiple interacting partners of the VIH2 were identified with their possible role in the biosynthesis of cell-wall structural proteins or in membrane plasticity. Therefore, we

speculated that VIH2 protein could modulate the cell-wall composition. To address this, we measured the different cell-wall components of control and transgenic *Arabidopsis* using standard methods that resulted in comparable yields and without starch interference. Our analysis indicated a consistent increase in the accumulation of cellulose (from 1.3 to 2.5-fold) in the transgenic lines that was consistent among the biological replicates and multiple transgenic lines. Additionally, arabinoxylan (AX) and arabinogalactan (AG) was also increased (1.8- 2.2 and 1.47- 1.5-fold) in the transgenic lines as compared to the controls (Supplementary Table S4). Our extraction procedures for control plants show the ratio of 1::1.2 to 1.5 for arabinose/galactose and arabinose/xylans, this validates our extraction procedures. To further validate the role of VIH proteins, *Atvih2-3* mutant line was used for measuring the biochemical composition of the shoots cell wall. Our analysis showed a significant reduction of the AG, AX and cellulose content in this mutant line (Figure 9D). Altogether, our data demonstrate that overexpression of wheat VIH resulted in the compositional change in the cell-wall biosynthesis-related sugars and these changes could be linked to the enhanced drought response in leaves.

Discussion

Recently, studies investigating inositol pyrophosphates have gained much attention due to the presence of high energy pyrophosphate moieties speculated to regulate metabolic homeostasis in organisms [16,17,26–28]. This study was performed to characterize and identify the functional mechanism of VIH proteins involved in the biosynthesis of PP-InsPx. We have identified and characterized two wheat inositol pyrophosphate kinase (TaVIH1 and Ta VIH2) encoding genes and demonstrated that homoeolog *TaVIH2-3B* interacts with cell wall related proteins. Overexpression of TaVIH2 in *Arabidopsis* could enhance growth and provide tolerance to drought stress by modulating cell-wall and ABA related proteins through altered cell-wall polysaccharide composition (AG, AX and cellulose).

Hexaploid bread wheat has one of the most complex genomes comprising of three related sub-genomes that have originated from three separate diploid ancestors thus forming an allohexaploid genome [29,30]. Therefore, to consider the appropriate homoeolog-transcript for further studies, Wheat-Exp expression database was used to analyse VIH2 homoeolog expression in different tissues and also during the developmental time course (Figure S2). VIH2 is known to be involved in defense response via a jasmonate-dependent resistance in Arabidopsis [17]. Wheat VIH genes were also induced upon infection of plants with pathogens (Supplementary Figure S2). Thus, the role of plant VIH genes during plant-microbe interaction

was found to be conserved. TaVIH protein was authentic kinase protein since its kinase domain could catalyse the phosphorylation and harbors yeast VIP1-like activity as demonstrated by its utilization of both IP_6 and IP_7 as potential substrates. In the past, *AtVIH* genes have been shown to be biochemically active for kinase activity that generates $InsP_7$ and $InsP_8$ [16,17]. Similarly, yeast and human enzymes also show IP_6 and IP_7 kinase activity [13,31,32].We propose that additional studies needs to be performed in future to confirm the chemical-forms of IP_7 and IP_8 generated by TaVIH2 using Nuclear Magnetic Resonance spectroscopy. TaVIH2-3B showed the highest homology to AtVIH2 (70.6 %).

The presence of various *cis*-acting elements in the promoter region plays essential roles in transcriptional regulation of genes in response to multiple environmental factors. The transcriptional activity of *TaVIH2* promoter and differential expression analysis link TaVIH2 with Pi-starvation response (Figure S2). This function of inositol pyrophosphate kinases in the regulation of Pi homeostasis seems to be evolutionarily conserved [28,32]. Very recently in *Arabidopsis*, it was demonstrated that VIH derived $InsP_8$ is required to sense the cellular Pi status and also binds to the intracellular Pi sensor SPX1 to control Pi homeostasis in plants [33]. We found that in addition to Pi homeostasis, *TaVIH2* promoter also responds to drought conditions. Y2H study led to the identification of TaFLA6 and multiple cell-wall reinforcement proteins as potential interactions of plant VIH proteins. Our qRT-PCR specifically indicates that both *TaVIH2* and *FLA6* are co-expressed under drought condition, suggesting that they are involved in the similar post-transcriptional response pathway (Supplementary Figure S8). Previously, it was shown that FLA proteins were involved in cell-wall reinforcement, plasticity, cell to cell adhesion and drought tolerance [22,34–37]. Cereal grains such as wheat are also rich in arabinogalactans such as FLA[38] indicating that associated VIH proteins might be responsible for these physiological responses including late stages of grain maturation (Figure 1C).

The high numbers of reoccurring clones related to the cell wall biosynthesis suggest an important role that VIH proteins may offer during developmental stages. Previously, multiple *Arabidopsis* FLA proteins were reported to be perturbed under drought conditions [39,40]. FLA-like protein was shown to be involved in molecular responses of Pi deficiency that is mediated by the induced root hair elongation [41]. The domain analysis of FLA6 suggests it belonged to the category-IV of FLAs and show presence of all the necessary domains, typical of this gene family (Figure 6D). It is important to notice that additional VIH2 interacting clones encode for glycosyltransferases, xylan-arabinosyl transferase and glycine-rich cell-wall structural like-protein. Surprisingly, genes encoding for glycosyltransferases, xylan-arabinosyl transferases

406 are homoeologs (*TaGT* and *TaXat*) and belong to the family of transferases. The glycosyl and
407 xylan arabinosyl transferases are involved in the biosynthesis of polysaccharides for cell-wall
408 [42,43]. Similarly, glycine-rich cell-wall proteins are recognized for their role in cell-wall
409 reinforcement by callose deposition [44].

410 Protein-protein interaction studies could provide associated functional clues. Yeast
411 VIP1 was shown to interact with histone H3/H4 chaperone, ASF1. VIP1 and ASF1
412 counterparts in *S. pombe* functionally regulate actin-related protein-2/3 complexes and thereby
413 participate in the fate of cell morphology [19]. Protein-protein interaction studies using human
414 PPIP5K1 identified multiple proteins involved in vesicle-mediated trafficking, lipid
415 metabolism and cytoskeletal organization [45]. This protein interaction has been accorded to
416 the presence of long C-terminal intrinsic disorder region (IDR) of PPIP5K1. Here, in case of
417 wheat VIH2 18.59 % of the predicted disorder content was observed that reflect the presence
418 of IDR boundaries[46]. Presence of such IDR in VIH2 could support interaction with cell-wall
419 scaffolding proteins, akin to the interaction ability of human PPIP5K1 [45,47].

420 Earlier the double mutants of VIH genes in *Arabidopsis* show severe growth defects,
421 implicating their unexplored role in overall growth and development[18]. We hypothesize that
422 the molecular and biochemical changes in transgenic *Arabidopsis* provide the overall
423 mechanical strength to the plant cell and in turn tolerance to stress condition. These
424 observations were also supported by our transcriptome analysis of two independent TaVIH2
425 overexpressing *Arabidopsis* lines that show consistent high expression of cell-wall, ABA and
426 drought related genes (Figure 8 and Figure 9B). Multiple genes were differentially regulated
427 by full length TaVIH2 overexpression. This suggest that high protein levels of VIH2 could
428 cause changes in gene expression pattern. Classically, VIH proteins contains evolutionarily
429 conserved two distinct domains including a N terminal rimK/ATP GRASP kinase and
430 phosphatase domain. It remains to be dissected if the change in transcriptome response in these
431 transgenic *Arabidopsis* is due to the kinase or phosphatase domain. Earlier, multiple inositol-
432 1,3,4 tris*kis*phosphate 5/6-kinase (devoid of phosphatase domain) were also implicated for their
433 role in drought tolerance [48,49]. This may suggest that the tolerance for the drought could arise
434 by the presence of functional kinase domain.

435 Multiple studies have implicated that enhanced level of ABA leads to drought tolerance
436 [50]. The elevated levels of ABA in our transgenic plants could be the reason for the high
437 expression of genes for cell wall maintenance and biosynthesis. Cell wall related remodelling
438 and ABA regulated signalling are the primary response against abiotic stress including drought
439 [51–53]. ABA dependent increased expression of *CYP*s and *DREBP* have been reported earlier in

plants with their role implicated in drought stress [50,54,55]. Our study shows high basal expression of genes encoding for DREBP and CYPs. The constitutive high expression of these gene families in our transgenic *Arabidopsis* could account for their better adaptability for drought stress. Earlier, changes in cellular levels of $InsP_7$ and $InsP_8$ have been attributed to guard cell signalling, ABA sensitivity and resistance to drought in maize *mrp5* mutants [28,56]. This suggests a molecular link between VIH, ABA levels and drought resistance.

Atvih2-3 mutant lines lacking mRNA expression also show alteration in the cell wall composition despite its typical growth as wild type Col-0 (Figure 9D). Interestingly, *vih1* and *vih2* double mutants display severe growth defect that was rescued by the gene complementation [18]. Our overexpression data showing enhanced branching and robust growth collectively reinforce the notion that VIH are also involved in providing support for plant growth. The *vih2* mutant in *Arabidopsis* are more susceptible to infestation by caterpillar (*Pieris rapae*) and thrips [17]. The resistance against herbivore pathogens such as *P. rapae*, could be gained by modulating the genes associated with cell-wall modification [57]. *Arabidopsis VIH2* mutant lines showed compositional changes in the cell-wall extracted polysaccharides especially in the AG level. The decreased resistance in *vih2* mutants against herbivores could be accounted for the defect in signalling pathway via COI1-dependent gene regulation and changes in the structural composition of the cell-wall.

Taken together we propose a working model, where wheat VIH participate in the drought resistance in plants by modulating the changes in cell-wall gene expression, enhanced ABA levels and change in biochemical composition to provide more mechanical strength (Figure 10). In future, it will be interesting to quantitate the level of higher inositol pyrophosphates in these plants. In summary, our work along with the previous functional reports suggested an emerging novel role of plant VIH proteins in cell wall scaffolding functions to provide resistance against drought stress.

Methods

Plant materials and growth conditions

The experimentation in this study was conducted using Bread wheat (*Triticum aestivum* L.) variety C306, a rain-fed cultivar which is well known for its better processing quality. For collection of the tissue materials, the spikes were tagged at the first day after anthesis (DAA). Samples were collected in the form of spikes at 7, 14, 21 and 28 DAA stages and various tissues, including root, stem, leaf and flag leaf at 14 DAA stage respectively. To further dissect

the expression levels in spikelet's, 14 DAA seed was used to separate different tissues, including aleurone, endosperm, embryo, glumes and rachis as done previously [58].

All the experiments for the stress conditions were performed in three biological replicates. Wheat seeds were surface sterilized as described earlier [58] and were allowed to germinate on Whatman filter paper soaked with water for 3-5 days. The germinated seedlings (8-10) with their residual endosperm excised, were transferred to Hoagland's nutrient media in phytaboxes. For phosphate starvation (-Pi) experiment, seven days old seedlings were subjected to Pi-sufficient (+Pi) or -Pi nutrient condition as described previously [58]. The root and shoot samples were harvested at four different stages: 5, 10, 15 and 20 days of starvation and snap frozen. For drought stress experiment, the seedlings were allowed to grow in Hoagland's media containing 5% PEG-8000 [59]and samples collected 72 hrs after stress treatment. The hydroponic culture was carried out in a growth chamber set at 22 ± 1 °C, 50–70 % relative humidity and a photon rate of 300 µmol photons m^{-2} s^{-1} with a 16 h light/8 h dark cycle.

Isolation of total RNA, cDNA synthesis and quantitative real time PCR analysis

Total RNA from various tissues was extracted by manual method using TRIzol® Reagent (Invitrogen™). The integrity of RNA and concentration was measured and contamination of genomic DNA was removed by subjecting the RNA samples to DNase treatment using TURBO™ DNase (Ambion, Life Technologies). 2µg of total RNA was used for cDNA preparation using The Invitrogen SuperScript III First-Strand Synthesis System SuperMix (Thermo Fisher Scientific) as per the manufacturer's guidelines.

In order to quantify the gene expression, qRT-PCR was performed using the QuantiTect SYBR Green RT-PCR Kit (Qiagen, Germany). The gene specific primers capable of amplifying 150-250 bp region from all the three homoeologous of both *TaVIH* genes were carefully designed using Oligocalc software. Four technical replicates for each set of primers and minimum of two to three experimental replicates were used to validate the experiment. Gene specific primer (with similar primer efficiencies) used in the study are listed in Supplementary Table S6. ADP-ribosylation factor gene (*TaARF*) was used as an internal control in all the expression studies. The Ct values obtained after the run were normalized against the internal control and relative expression was quantified using $2^{-\Delta\Delta C_T}$ method [60]. For In-silico expression for *TaVIH* genes in different tissues and stresses, wheat VIH RefSeq IDs were used to extract expression values as TPMs from expVIP database. For different tissues and stages, the expression values were used to build a heatmap. In case of abiotic and biotic

stress conditions, the expression values from the control and stressed conditions were used to get fold change values, which were then used to plot heatmaps using MeV software.

Identification and cloning of two wheat VIH genes

Two *Arabidopsis* (AT5G15070.2 and AT3G01310.2) and the previously reported yeast VIP1 sequences were used to perform Blastx analysis against the IWGSC (www.wheatgenome.org/) and wheat EST databases. The identified EST sequences were checked for the presence of the typical dual domain structure. Further, screening of these sequences resulted in the identification of two different genomic locations (Table S1). Furthermore, the Pfam domain identifiers of the signature ATP-Grasp Kinase (PF08443) and Histidine Acid Phosphatase (PF00328) domains were used to identify VIH proteins in Ensembl database using BioMart application. The corresponding predicted homoelogous transcripts were identified and compared to the other VIH sequences. DNA STAR Lasergene 11 Core Suite was used to perform the multiple sequence alignment and to calculate the sequence similarity. Gene specific primers capable of amplifying the transcript from the specific genome was designed after performing 5`and 3`-RACE to ascertain the completed open reading frame (ORF). Subsequently, full length primers were designed to amplify the *VIH* genes. The generated full-length sequence information was further used for qRT-PCR related studies.

Homology modelling, hydropathy plot and IDR prediction

Homology modelling was performed for VIH1-4D & VIH2-3B based on their ATP-grasp domains (residues 7 to 332 for VIH1-4D and 12 to 339 for VIH2-3B), which share an identity of ~57% with hPPIP5K2 (residues 41 to 366). In both cases, the align2d command in MODELLER [61](V9.21) was used to align TaVIHs against hPPIP5K2 and the 3D models with ANP, IHP and 4 Mg^{2+} ions fitted in were calculated using the automodel class. Best models were selected based on the MODELLER objective function. The models were visualized using UCSF Chimera [62]. The hydropathy profile for proteins was calculated according to Kyte and Doolittle., 1982. The positive values indicate hydrophobic domains and negative values represent hydrophilic regions of the amino acid residues. To identify the % similarity with IDR boundaries, MFDp2 (http://biomine.cs.vcu.edu/servers/MFDp2 was used to predict the disorder content in the input sequence [46].

Construct preparation for expression vector and yeast functional complementation

For complementation assays, pYES2, a galactose-inducible yeast expression vector was used. The functional complementation of yeast by TaVIH proteins was studied using 6-azauracil based assay. The wild type BY4741 (MATa; his3D1; leu2D0; met15D0; ura3D0) and *vip1Δ* (BY4741; MATa; ura3Δ0; leu2Δ0; his3Δ1; met15Δ0; YLR410w::kanMX4) yeast strains were used for the growth assays. The CDS corresponding to the catalytic domain of *ScVIP1* (1-535 amino acids) cloned into pYES2 expression vector was used as a positive control. *TaVIH1/2* along with *ScVIP1* and empty vector were transformed individually into wild type and mutant strains by lithium acetate method with slight modifications. For growth assay, the wild type and mutant *S. cerevisiae* strains carrying different plasmids were allowed to grow overnight in minimal media without uracil. The primary culture was used to re-inoculate fresh media to an OD_{600} of 0.1 and allowed to grow till the culture attained an optical density of 0.6-0.8. The cell cultures were then adjusted to O.D of 1 and further serially diluted to the final concentrations of 1:10, 1:100 and 1:1000. 10 µl each of these cell suspensions were used for spotting on SD(-Ura) plates containing 2% galactose, 1% raffinose and varying concentrations of 6-azauracil (0, 2.5 and 5 mM). The colony plates were incubated at 30ºC and pictures were taken after 4 days.

Protein expression of wheat VIH1 and VIH2, In-Vitro Kinase assays, PAGE analysis and MADLI-Tof analysis

The TaVIH1-KD and TaVIH2-KD kinase domain was cloned and expressed in *E. coli* BL21 cells using 0.5 mM IPTG and lysis buffer having pH 7.4 containing 50 mM sodium phosphate, 300 mM NaCl and protein inhibitor cocktail. Post sonication and centrifugation purification was done on Cobalt resin affinity chromatography column (ThermoFisher Scientific, Waltham, MA, USA). After column saturation overnight at 4°C it was washed with washing buffer containing 7.5 mM imidazole and subsequently eluted with elution buffer containing 100 mM EDTA. The eluate was pooled and concentrated using a concentrator having a molecular weight cut-off of 10 kDa by spinning at conditions mentioned in the concentrator's manual. The concentrated enzyme preparation was washed thrice with sodium phosphate buffer and finally concentrated in Tris-HCl buffer, pH 7.4. To check expression western was done by using Mouse anti-HIS primary antibody and Goat Anti-Mouse secondary antibody [HRP IgG (H + L): 1:5000 dilutions; Invitrogen].

TaVIH1 and TaVIH2 kinase assays were performed in 20 mM HEPES (pH 7.5), 5 mM $MgCl_2$, 20 mM ATP, 2 mM IP_6 and 1 mM DTT with 30 ng of respective protein. ScVIP1 was taken as a control. The reaction was incubated at 28°C for 8-9 hrs, separated by PAGE and visualized by toluidine blue. Inositol polyphosphates were resolved using 18 cm gel using 33.3

% polyacrylamide gel in Tis-Borate EDTA as mentioned earlier [21]. Gels were pre-run for 75 min at 300 volts and samples were loaded mixed with Dye (10 mM TrisHCl pH 7.0; 1 mM EDTA; 30 % glycerol; 0.08 % Orange G). Gels were run at 5-6 mA for overnight at 4°C until the Orange G dye front reached 6 cm from the bottom of the gel. Bands were visualized by toluidine blue (0.1 % w/v) stain. TBE-PAGE gel purified products of TaVIH reaction was used for MALDI-ToF-MS analysis. MALDI-ToF-MS was performed from gel extract solutions which were pipetted on a α-Cyano-4-hydroxycinnamic acid (≥98%, Sigma) prepared on a stainless-steel plate (0.5 µL of a 10 mg/mL ACN/H2O 1:1 solution). Negative ionization mode was used for acquiring spectra on spectrometer (AB SCIEX TOF/TOF™ 5800; equipped with a 337 nm laser) operating in the linear mode.

Wheat cDNA Library construction, yeast two-hybrid screening and pull-down assays

The total RNA (~120 µg) samples were pooled from the vegetative tissues including shoots and roots. From the isolated total RNA, mRNA purification was performed by using (NucleoTrap mRNA mini kit, Macherey-Nagel, Germany). A total of 0.25 µg mRNA was used to make the cDNA library (Make & Plate™ Library System, Clontech, USA). The wheat cDNA library was prepared and purified using CHROMA SPIN+TE-400 columns. A cDNA fragment sizes of <2kb was used for the library screening using TaVIH2 as a bait. The library shows the titre value of ~$0.8x10^9$ cfu/ml. Yeast two-hybrid assays and screening were performed by using GAL4-based screening system (Matchmaker Gold Yeast Two-hybrid System, Takara Inc., USA). Most of the steps were followed as per manufacturer's instructions unless mentioned. Briefly, putative positive interacting clones were obtained when the competent yeast strain Y187 was co-transformed with cDNA library+AD (pGADT7-Rec vector) and Y2H-Gold containing BD vector (*TaVIH2-3B:pGBKT7* bait vector) respectively. Following stringent screening procedures, putative clones were obtained and screened for their reporter assays (Aureobasidin A). Full length ORF was cloned for the gene of interest and one-on-one interaction was also done to confirm its interaction. Routine yeast transformation was done by using Yeastmaker Yeast transformation System 2 (Clontech, USA).

Yeast cell lysate was prepared for performing pull down assay by using glass bead in buffer (1% SDS, 100mM NaCl,100mM Tris-Cl, 1mM EDTA, 2% Triton and 1mM protease inhibitor (100X Halt protease inhibitor, Thermofisher, USA). The protein concentration in lysate was calculated at two dilutions and processed further using 2 ul of anti-c-Myc antibody. The proteins were transfer to PVDF membrane and the blot was separated into two parts to detect TaVIH2 and TaFLA6 respectively. Different primary antibodies were used for probing

(mouse Anti-c-myc and rabbit anti-HA with 1:2000 dilution). After washing the blots with TBST, they were treated with the secondary antibody (Goat Anti-Mouse IgG (H + L); and Goat Anti-Rabbit IgG (H + L) with 1:5000 dilution. Blot was developed by using BIO-RAD clarity western ECL Substrate.

Protein localization

For the localization experiments *TaFLA6* was cloned in pGADT7 vector at *Eco*R1 and *Bam*H1 sites. *TaVIH2* cDNA was cloned in pGBKT7 vector using *Sma*1 and *Not*1 restriction sites. The constructs were transformed in Y2H Gold yeast strain and selected on SD-Leu or SD-Trp plates respectively. Yeast spheroplasts were prepared for localization study. Mouse monoclonal Anti-HA (HA:FLA6-pGADT7): or rabbit Anti-c-Myc (cMYC:VIH2-pGBKT7) primary antibody (Invitrogen, USA) was used for the respective preparations, at a ratio of 1:200 followed by 5 washing with blocking buffer. Yeast cells were incubated with Goat Anti- Mouse IgG (H+L) Alexa Flour Plus 488 or Goat Anti- Rabbit IgG (H+L) Alexa Flour Plus 647 (Invitrogen, USA) at a ratio of 1:500 for 4hr at room temperature. Cells were washed with blocking buffer and mounted with Fluor mount (Sigma, USA). Representative fluorescent images were taken using Zeiss fluorescence microscope Axio Imager Z2 with an Axiocam MRm camera at 63X of magnification.

Cloning of VIH promoter, cDNA and *Arabidopsis* transformation

For promoter, ~2000 bp fragments upstream of the start codon were PCR amplified from genomic DNA of cv. C306. The cloned DNA fragments (in pJET1.2) were sequenced confirmed and inserted into pCAMBIA1391z, a promoter-less binary vector containing GUS reporter gene, using forward and reverse primers with Bam*HI* and Nco*I* sites respectively to form a *TaVIHpromoter:GUS* in pCAMBIA1391z. The promoter sequences of *TaVIH* genes were analysed for the presence of cis-regulatory elements using PLANTCARE database (http://bioinformatics.psb.ugent.be/webtools/plantcare/). For VIH2 cDNA (~3117 bp), blunt ended cloning was done at *Spe*1 generated site in pCAMBIA1302 along with the C-terminal His (pCAMBIA1302:*TaVIH*-His) tag. The generated transcription units were introduced into *Arabidopsis* seedlings using *Agrobacterium* mediated transformation by floral dip method [63]. Three to four weeks old plants grown at 22 ± 1 °C, 16 h light/8 h dark cycle and a photon rate of 100 µmol photons m^{-2} s^{-1} were used for transformation. The independent transformants were screened on 0.5X MS media containing 30 mg/L hygromycin and 0.8% agar. The transformed seedlings with long hypocotyls and green expanded leaves at 4-leaf stage were

separated out from the non-transformed seedlings and transferred to soil after about 3 weeks. In a similar manner T_1 and T_2 generation seeds were also selected and allowed to grow till maturity. The transgenic seedlings were confirmed for the presence of recombinant cassette using PCR based approach. The transgenic lines harbouring empty pCAMBIA1391Z or pCAMBIA1302 vector was used as respective negative control. The PCR positive lines were further used for functional characterization.

GUS-reporter assays and characterization of transgenic lines *in Arabidopsis*

For promoter analysis, the seeds of PCR positive lines were surface sterilized and grown on 0.5X MS (Murashige and Skoog media) agar plates containing 30 mg/L Hygromycin B for 15 days before they were subjected to various abiotic stress and hormonal treatments. For dehydration stress, the seedlings were air dried by placing them on Whatman filter paper for 1hr. Heat treatment was given by incubating the seedlings at 37˚C for 8hrs. Exposure to ABA (100 µM), GA_3 (20 µM), NaCl (300 mM) and drought (20% and 30% PEG) were given by placing the seedlings on filter paper impregnated with 0.5X MS solution containing the respective chemical for 24 hrs. For Pi deficiency, seedlings were allowed to grow on 0.5X MS agar plates without KH_2PO_4 for 96 hrs. Histochemical staining of seedlings after respective treatments were performed by incubated overnight in GUS staining solution [64] with 2 mM X-Gluc (5-bromo-4-chloro-3-indolyl-beta-D-glucuronic acid, HiMedia, India) at 37 ˚C in a 48-well microplate containing about ten seedlings/well. Chlorophyll was removed from tissues by dipping in 90% ethanol. The staining was visualized and photographed under Leica DFC295 stereomicroscope (Wetzlar, Germany) at magnification of 6.3X. MS solution without any chemical served as a control.

For characterization of transgenic lines overexpressing VIH proteins parameters such as rosette area, number of leaves, leaves size, length of main root axis and number of shoots (primary and secondary). Four independent confirmed homozygous transgenic lines were used for this study. Each parameter was calculated using three experimental replicates, each consisting of twelve plants. For stress experiments, three days old seedlings of transgenic and control pre-grown on 0.5X MS were transferred to 0.5X MS plates consisting of either 125 mM mannitol or 10 % glycerol for mimic drought condition. Ten seedlings were used and the experiments were repeated for three times with similar phenotype. For control, seedlings continued to grow on ½ MS plates. Root lengths were measured and graphs were plotted (using three experimental replicate) and pictures were taken after nine days of growth. To calculate the relative water loss %, twenty-five leaves per five plants with similar developmental stage

for each of the transgenic lines and control plants were subjected to incubation (27 ˚C) for the period of 12 hrs. Fresh weight of the detached leaf was taken and continued for the measurements after every 2 hrs. The experiment was repeated twice with similar observations. For drought response minimum of fifty-five seedlings were pre-grown for the period of fourteen days and were subjected to drought for additional fourteen days. The plants were then re-watered for the period of seven days and % survival rates were calculated.

RNAseq profiling

Col-0(Ev) and overexpressing *TaVIH2-3B* Arabidopsis (#Line4 and 6) seedlings were grown for the period of 25 days. For each genotype, total RNA was extracted from three independent biological replicates by using RNeasy Plant Mini Kits (Qiagen, CA). Genomic DNA contamination was removed by digestion with Turbo DNase (BioRad, CA). RNA quantity was checked by Bioanalyzer for quality control (RIN>8). Library construction and sequencing were performed by Eurofins, Bangalore, India; using pair end library preparation. About 9.5 to 13.8 million raw reads were obtained for each sample. Raw reads were processed to filter out the adapter and low quality (QV<20) reads using trimmomatic v0.39 [65] which were then pseudo-aligned against the reference transcriptome (ensembl release 48) using kallisto v0.46.2 [66]. The obtained raw abundances were summarized to gene-level expression counts using tximport and imported to DESeq2 [67,68] for differential expression (DE) analysis in R. The obtained log2 fold change (LFC) values were further processed using apeglm package to reduce noise [18].Genes with 1 > LFC < -1 and padj < 0.05 were considered significantly DE. The expression correlation across lines and within replicates was analyzed using Principal Component Analysis (PCA) in ggplot2 [69] .

GC-MS analysis of Arabidopsis cell wall polysaccharides and ABA measurement

Extraction of cell wall components was performed as described earlier with minor modification as depicted in the flowchart as Supplementary Figure S11 [70]. Since such chemical analysis requires relatively large amounts of samples, pools from 3-5 independent plants (for each of the three biological replicates) of the respective lines expressing wheat VIH2 were used for chemical analysis. Briefly, five grams (fresh weight) of shoots from respective lines and control at similar developmental stages (~25 days old) was crushed to a fine powder and processed further. The derived pellet was used for extraction of Arabinoxylan (AX) and Cellulose; whereas the supernatant was used for extracting arabinogalactan (AG). The extractions were checked with Iodine solution to make sure that they are free of starch interference. The

compositional analysis the extracted AG, AX and Cellulose were determined by preparing their alditol derivatives and processed for gas chromatography–mass spectrometry (GC-MS) analysis as described [71,72]. Two µl of samples were introduced in the split less injection mode in DB-5 (60 m × 0.25 mm, 1 µm film thickness, Agilent, CA) using helium as a carrier gas. The alditiol acetate derivative was separated using the following temperature gradient: 80 °C for 2 min, 80-170 °C at 30°C/min, 170-240 °C at 4°C/min, 240 °C held for 30 min and the samples were ionized by electrons impact at 70 eV. ABA was measured using Plant Hormone Abscisic Acid (ABA) ELISA kit (Real Gene, Germany). Twenty-five days old plants leaves were used for the measurement of the ABA content. One gram of fresh weight form eight plants for each line was used for extractions. The experiments were repeated with at least three independent extractions and concentration was calculated using standard graphs as per the manual instructions. Standard graph was plotted using Log of concentration and colour development for each line was measured at 430 nm (Supplementary Figure S12).

Acknowledgements

Authors thank Executive Director for facilities and support. This study was supported by Department of Biotechnology, Basic Plant Biology Grant to AKP [BT/PR12432/BPA/118/35/2014]. Part of this work was also supported by NABI-CORE grant to AKP. Yeast strain *vip1Δ* and ScVIP1-cDNA was kindly gifted by Dr. Rashna Bhandari (CDFD). MK thank UGC-CSIR for her research scholarship. Thanks to Dr. Gabriel Schaff for sharing the *Arabidopsis vih2-3* mutant. AS thank DBT for SRF fellowship. DBT-eLibrary Consortium (DeLCON) is acknowledged for providing timely support and access to e-resources for this work.

Data availability

The resources including plasmids, constructs and transgenic *Arabidopsis* seeds will be available upon request.

References:

1. Stephens, L. *et al.* The detection, purification, structural characterization, and metabolism of diphosphoinositol pentakisphosphate(s) and bisdiphosphoinositol tetrakisphosphate(s). *J. Biol. Chem.* **268**, 4009–4015 (1993).
2. Luo, H. R. *et al.* Inositol pyrophosphates are required for DNA hyperrecombination in protein kinase c1 mutant yeast. *Biochemistry* **41**, 2509–15 (2002).
3. Dubois, E. *et al.* {InSaccharomyces} cerevisiae, the Inositol Polyphosphate Kinase Activity of Kcs1p Is Required for Resistance to Salt Stress, Cell Wall Integrity, and

Vacuolar Morphogenesis. *J. Biol. Chem.* **277**, 23755–23763 (2002).
4. Saiardi, A., Bhandari, R., Resnick, A. C., Snowman, A. M. & Snyder, S. H. Phosphorylation of proteins by inositol pyrophosphates. *Science (80-.).* **306**, 2101–2105 (2004).
5. Norman, K. L. *et al.* Inositol polyphosphates regulate and predict yeast pseudohyphal growth phenotypes. *PLoS Genet.* **14**, e1007493 (2018).
6. Auesukaree, C., Tochio, H., Shirakawa, M., Kaneko, Y. & Harashima, S. Plc1p, Arg82p, and Kcs1p, Enzymes Involved in Inositol Pyrophosphate Synthesis, Are Essential for Phosphate Regulation and Polyphosphate Accumulation {inSaccharomyces} cerevisiae. *J. Biol. Chem.* **280**, 25127–25133 (2005).
7. Wilson, M. S., Jessen, H. J. & Saiardi, A. The inositol hexakisphosphate kinases IP6K1 and -2 regulate human cellular phosphate homeostasis, including XPR1-mediated phosphate export. *J. Biol. Chem.* **294**, 11597–11608 (2019).
8. Voglmaier, S. M. *et al.* Purified inositol hexakisphosphate kinase is an ATP synthase: Diphosphoinositol pentakisphosphate as a high-energy phosphate donor. *Proc. Natl. Acad. Sci. U. S. A.* **93**, 4305–4310 (1996).
9. Saiardi, A., Erdjument-Bromage, H., Snowman, A. M., Tempst, P. & Snyder, S. H. Synthesis of diphosphoinositol pentakisphosphate by a newly identified family of higher inositol polyphosphate kinases. *Curr. Biol.* **9**, 1323–1326 (1999).
10. Draškovič, P. *et al.* Inositol Hexakisphosphate Kinase Products Contain Diphosphate and Triphosphate Groups. *Chem. Biol.* **15**, 274–286 (2008).
11. Choi, J. H., Williams, J., Cho, J., Falck, J. R. & Shears, S. B. Purification, Sequencing, and Molecular Identification of a Mammalian {PP}-{InsP}5Kinase That Is Activated When Cells Are Exposed to Hyperosmotic Stress. *J. Biol. Chem.* **282**, 30763–30775 (2007).
12. Fridy, P. C., Otto, J. C., Dollins, D. E. & York, J. D. Cloning and characterization of two human VIP1-like inositol hexakisphosphate and diphosphoinositol pentakisphosphate kinases. *J. Biol. Chem.* **282**, 30754–62 (2007).
13. Mulugu, S. *et al.* A conserved family of enzymes that phosphorylate inositol hexakisphosphate. *Science (80-.).* **316**, 106–109 (2007).
14. Dorsch, J. A. *et al.* Seed phosphorus and inositol phosphate phenotype of barley low phytic acid genotypes. *Phytochemistry* **62**, 691–706 (2003).
15. Lemtiri-Chlieh, F., MacRobbie, E. A. C. & Brearley, C. A. Inositol hexakisphosphate is a physiological signal regulating the K$\mathplus$-inward rectifying conductance in guard cells. *Proc. Natl. Acad. Sci.* **97**, 8687–8692 (2000).
16. Desai, M. *et al.* Two inositol hexakisphosphate kinases drive inositol pyrophosphate synthesis in plants. *Plant J.* **80**, 642–653 (2014).
17. Laha, D. *et al.* VIH2 Regulates the Synthesis of Inositol Pyrophosphate InsP8 and Jasmonate-Dependent Defenses in Arabidopsis. *Plant Cell* **27**, 1082–97 (2015).
18. Zhu, J. *et al.* Two bifunctional inositol pyrophosphate kinases/phosphatases control plant phosphate homeostasis. *Elife* **8**, (2019).
19. Osada, S. *et al.* Inositol phosphate kinase Vip1p interacts with histone chaperone Asf1p in Saccharomyces cerevisiae. *Mol. Biol. Rep.* **39**, 4989–4996 (2011).
20. Borrill, P., Ramirez-Gonzalez, R. & Uauy, C. expVIP: A customizable RNA-seq data analysis and visualization platform. *Plant Physiol.* **170**, 2172–2186 (2016).
21. Losito, O., Szijgyarto, Z., Resnick, A. C. & Saiardi, A. Inositol pyrophosphates and their unique metabolic complexity: analysis by gel electrophoresis. *PLoS One* **4**, e5580–e5580 (2009).
22. Johnson, K. L., Jones, B. J., Bacic, A. & Schultz, C. J. The Fasciclin-Like Arabinogalactan Proteins of Arabidopsis. A Multigene Family of Putative Cell

Adhesion Molecules. *Plant Physiol.* **133**, 1911–1925 (2003).

23. Gillmor, C. S. *et al.* Glycosylphosphatidylinositol-Anchored Proteins Are Required for Cell Wall Synthesis and Morphogenesis in Arabidopsis. *Plant Cell* **17**, 1128–1140 (2005).
24. Schultz, C., Gilson, P., Oxley, D., Youl, J. & Bacic, A. {GPI}-anchors on arabinogalactan-proteins: implications for signalling in plants. *Trends Plant Sci.* **3**, 426–431 (1998).
25. Saha, S., Anilkumar, A. A. & Mayor, S. GPI-anchored protein organization and dynamics at the cell surface. *Journal of Lipid Research* vol. 57 159–175 (2016).
26. Chakraborty, A., Kim, S. & Snyder, S. H. Inositol pyrophosphates as mammalian cell signals. *Science Signaling* vol. 4 (2011).
27. Jadav, R. S., Chanduri, M. V. L., Sengupta, S. & Bhandari, R. Inositol Pyrophosphate Synthesis by Inositol Hexakisphosphate Kinase 1 Is Required for Homologous Recombination Repair. *J. Biol. Chem.* **288**, 3312–3321 (2012).
28. Williams, S. P., Gillaspy, G. E. & Perera, I. Y. Biosynthesis and possible functions of inositol pyrophosphates in plants. *Front. Plant Sci.* **6**, (2015).
29. Huang, S. *et al.* Genes encoding plastid acetyl-CoA carboxylase and 3-phosphoglycerate kinase of the Triticum/Aegilops complex and the evolutionary history of polyploid wheat. *Proc. Natl. Acad. Sci. U. S. A.* **99**, 8133–8 (2002).
30. Dvorak, J. & Akhunov, E. D. Tempos of Gene Locus Deletions and Duplications and Their Relationship to Recombination Rate During Diploid and Polyploid Evolution in the Aegilops-Triticum Alliance. *Genetics* **171**, 323–332 (2005).
31. Choi, K., Mollapour, E. & Shears, S. B. Signal transduction during environmental stress: {InsP}8 operates within highly restricted contexts. *Cell. Signal.* **17**, 1533–1541 (2005).
32. Lee, Y. S., Mulugu, S., York, J. D. & O'Shea, E. K. Regulation of a cyclin-CDK-CDK inhibitor complex by inositol pyrophosphates. *Science (80-.).* **316**, 109–112 (2007).
33. Dong, J. *et al.* Inositol Pyrophosphate InsP8 Acts as an Intracellular Phosphate Signal in Arabidopsis. *Mol. Plant* **12**, 1463–1473 (2019).
34. Majewska-Sawka, A. & Nothnagel, E. A. The multiple roles of arabinogalactan proteins in plant development. *Plant Physiology* vol. 122 3–9 (2000).
35. Shi, H., Kim, Y. S., Guo, Y., Stevenson, B. & Zhu, J. K. The Arabidopsis SOS5 locus encodes a putative cell surface adhesion protein and is required for normal cell expansion. *Plant Cell* **15**, 19–32 (2003).
36. MacMillan, C. P., Mansfield, S. D., Stachurski, Z. H., Evans, R. & Southerton, S. G. Fasciclin-like arabinogalactan proteins: specialization for stem biomechanics and cell wall architecture in Arabidopsis and Eucalyptus. *Plant J.* **62**, 689–703 (2010).
37. Huang, G.-Q. *et al.* Characterization of 19 novel cotton FLA genes and their expression profiling in fiber development and in response to phytohormones and salt stress. *Physiol. Plant.* **134**, 348–59 (2008).
38. Nirmal, R. C., Furtado, A., Rangan, P. & Henry, R. J. Fasciclin-like arabinogalactan protein gene expression is associated with yield of flour in the milling of wheat. *Sci. Rep.* **7**, (2017).
39. No, E.-G. & Loopstra, C. A. Hormonal and developmental regulation of two arabinogalactan-proteins in xylem of loblolly pine (Pinus taeda). *Physiol. Plant.* **110**, 524–529 (2000).
40. Cagnola, J. I. *et al.* Reduced expression of selected {FASCICLIN}-{LIKE} {ARABINOGALACTAN} {PROTEIN} genes associates with the abortion of kernels in field crops of Zea mays (maize) and of Arabidopsis seeds. *Plant. Cell Environ.* **41**, 661–674 (2018).

41. Kirchner, T. W. *et al.* Molecular Background of Pi Deficiency-Induced Root Hair Growth in Brassica carinata {\textendash} A Fasciclin-Like Arabinogalactan Protein Is Involved. *Front. Plant Sci.* **9**, (2018).
42. Scheible, W.-R. & Pauly, M. Glycosyltransferases and cell wall biosynthesis: novel players and insights. *Curr. Opin. Plant Biol.* **7**, 285–295 (2004).
43. Whitehead, C. *et al.* A glycosyl transferase family 43 protein involved in xylan biosynthesis is associated with straw digestibility in Brachypodium distachyon. *New Phytol.* **218**, 974–985 (2018).
44. Ueki, S. & Citovsky, V. Identification of an interactor of cadmium ion-induced glycine-rich protein involved in regulation of callose levels in plant vasculature. *Proc. Natl. Acad. Sci. U. S. A.* **102**, 12089–94 (2005).
45. Machkalyan, G., Trieu, P., Pétrin, D., Hébert, T. & Miller, G. PPIP5K1 interacts with the exocyst complex through a C-terminal intrinsically disordered domain and regulates cell motility. *Cell. Signal.* **28**, (2016).
46. Mizianty, M. J. *et al.* Improved sequence-based prediction of disordered regions with multilayer fusion of multiple information sources. *Bioinformatics* **26**, i489–i496 (2010).
47. Randall, T. A., Gu, C., Li, X., Wang, H. & Shears, S. B. A two-way switch for inositol pyrophosphate signaling: Evolutionary history and biological significance of a unique, bifunctional kinase/phosphatase. *Adv. Biol. Regul.* **75**, 100674 (2020).
48. Marathe, A. *et al.* Exploring the role of Inositol 1,3,4-trisphosphate 5/6 kinase-2 (GmITPK2) as a dehydration and salinity stress regulator in Glycine max (L.) Merr. through heterologous expression in E. coli. *Plant Physiol. Biochem.* **123**, 331–341 (2018).
49. Du, H. *et al.* Characterization of an inositol 1,3,4-trisphosphate 5/6-kinase gene that is essential for drought and salt stress responses in rice. *Plant Mol. Biol.* **77**, 547–563 (2011).
50. Daszkowska-Golec, A. & Szarejko, I. The Molecular Basis of ABA-Mediated Plant Response to Drought. *Abiotic Stress - Plant Responses and Applications in Agriculture* (2013) doi:10.5772/53128.
51. Moore, J. P., Vicré-Gibouin, M., Farrant, J. M. & Driouich, A. Adaptations of higher plant cell walls to water loss: drought vs desiccation. *Physiol. Plant.* **134**, 237–245 (2008).
52. Tenhaken, R. Cell wall remodeling under abiotic stress. *Front. Plant Sci.* **5**, 771 (2015).
53. Takahashi, F., Kuromori, T., Urano, K., Yamaguchi-Shinozaki, K. & Shinozaki, K. Drought Stress Responses and Resistance in Plants: From Cellular Responses to Long-Distance Intercellular Communication. *Front. Plant Sci.* **11**, 556972 (2020).
54. Shinozaki, K. & Yamaguchi-Shinozaki, K. Gene networks involved in drought stress response and tolerance. *J. Exp. Bot.* **58**, 221–227 (2006).
55. Pandian, B. A., Sathishraj, R., Djanaguiraman, M., Prasad, P. V. V. & Jugulam, M. Role of Cytochrome P450 Enzymes in Plant Stress Response. *Antioxidants (Basel, Switzerland)* **9**, 454 (2020).
56. Klein, M. *et al.* The plant multidrug resistance ABC transporter AtMRP5 is involved in guard cell hormonal signalling and water use. *Plant Journal* vol. 33 119–129 (2003).
57. De Vos, M. *et al.* The arabidopsis thaliana transcription factor AtMYB102 functions in defense against the insect herbivore Pieris rapae. *Plant Signal. Behav.* **1**, 305–311 (2006).
58. Shukla, V. *et al.* Tissue specific transcript profiling of wheat phosphate transporter

genes and its association with phosphate allocation in grains. *Sci. Rep.* **6**, (2016).
59. Ji, H. *et al.* {PEG}-mediated osmotic stress induces premature differentiation of the root apical meristem and outgrowth of lateral roots in wheat. *J. Exp. Bot.* **65**, 4863–4872 (2014).
60. Livak, K. J. & Schmittgen, T. D. Analysis of Relative Gene Expression Data Using Real- Time Quantitative PCR and the 2 ☒☒ C T Method. *Methods* **408**, 402–408 (2001).
61. Eswar, N. *et al.* Comparative Protein Structure Modeling Using Modeller. *Curr. Protoc. Bioinforma.* **15**, 5.6.1--5.6.30 (2006).
62. Pettersen, E. F. *et al.* {UCSF} Chimera?A visualization system for exploratory research and analysis. *J. Comput. Chem.* **25**, 1605–1612 (2004).
63. Zhang, X., Henriques, R., Lin, S. S., Niu, Q. W. & Chua, N. H. Agrobacterium-mediated transformation of Arabidopsis thaliana using the floral dip method. *Nat. Protoc.* **1**, 641–646 (2006).
64. Jefferson, R. A. Assaying chimeric genes in plants: The GUS gene fusion system. *Plant Mol. Biol. Report.* **5**, 387–405 (1987).
65. Bolger, A. M., Lohse, M. & Usadel, B. Trimmomatic: a flexible trimmer for Illumina sequence data. *Bioinformatics* **30**, 2114–2120 (2014).
66. Bray, N. L., Pimentel, H., Melsted, P. & Pachter, L. Erratum: Near-optimal probabilistic RNA-seq quantification. *Nat. Biotechnol.* **34**, 888 (2016).
67. Love, M. I., Huber, W. & Anders, S. Moderated estimation of fold change and dispersion for RNA-seq data with DESeq2. *Genome Biol.* **15**, 550 (2014).
68. Soneson, C., Love, M. I. & Robinson, M. D. Differential analyses for RNA-seq: transcript-level estimates improve gene-level inferences. *F1000Research* **4**, 1521 (2015).
69. Gómez-Rubio, V. ggplot2 - Elegant Graphics for Data Analysis (2nd Edition). *J. Stat. Softw.* **77**, (2017).
70. Zablackis, E., Huang, J., Müller, B., Darvill, A. G. & Albersheim, P. Characterization of the cell-wall polysaccharides of Arabidopsis thaliana leaves. *Plant Physiol.* **107**, 1129–1138 (1995).
71. Blakeney, A. B., Harris, P. J., Henry, R. J. & Stone, B. A. A simple and rapid preparation of alditol acetates for monosaccharide analysis. *Carbohydr. Res.* **113**, 291–299 (1983).
72. Bhagia, S., Nunez, A., Wyman, C. E. & Kumar, R. Robustness of two-step acid hydrolysis procedure for composition analysis of poplar. *Bioresour. Technol.* **216**, 1077–1082 (2016).

List of Tables:

Table 1: List of genes identified as an interacting partners of wheat VIH2-3B. The table summarises the information of the predicted gene function (based on the ensemble-BLAST) of the sequenced clones. All the enlist genes resulted in blue colony formation when the screening was performed on the SD-GALα (-AHLT) plates. Respective TRIAE IDs (RefSeq V1.0) are

mentioned. Most of these genes show more than once occurrence of the yeast colonies during screening except for S.No 1, 2,3 clones that appeared more than thrice.

S.No	Predicted Biological Annotation	New TRIAE_ ID
1.	*Fasciclin-like arabinogalactan protein (FLA6) (protein ID:* ABI95396.1)	TraesCS2A02G165600
2.	*Glycosyl transferases (GT)*	TraesCS6B02G339100.1
3.	*Xylan arabinosyl transferase (Xat1)*	TraesCS6A02G309400.1
4.	*Glycine-rich cell-wall structural protein-like*	TraesCS2B02G541900
5.	*Alpha-amylase/trypsin inhibitor CM1*	TraesCS7B02G072000
6.	*NADH-ubiquinone reductase complex 1 MLRQ subunit;*	TraesCS7A02G238600
7.	*Hypothetical protein TRIUR3_12806*	TraesCS4A02G016700
8.	*ABC transporter B family member 25 A1-1*	TraesCS5A02G392600
9.	*Short chain dehydrogenase reductase*	TraesCS2B02G116700
10.	*WW domain binding protein (containing PPGPPP motif)*	TraesCS2A02G245500
11.	*Ethylene-responsive element binding protein 1 (EREB1) mRNA,*	TraesCS7B02G062200
12.	*Triticum aestivum mRNA, clone: tplb0058f16,*	TraesCS2A02G558900

Figure 1. Neighbourhood-Joining phylogenetic tree and expression analysis of wheat genes encoding VIH. (A) Neighbourhood-Joining phylogenetic tree of VIP proteins. The full-length amino acid sequences of VIH proteins from various taxonomic groups were used for the construction of phylogeny using MEGA7.0. (B) *TaVIH1* and *TaVIH2* in different tissues of a wheat plant. The cDNA prepared from 2µg of DNA free-RNA isolated from root, stem, leaf and flag leaf tissues of a 14 DAA plant as template. (C) Quantitative expression analysis of *TaVIH* genes at different seed maturation stages (7, 14, 21 and 28 days after anthesis and in 14

DAA seed (aleurone, Al; endosperm, En; embryo, Em; glumes, Gl and and rachis, Ra. For qRT-PCR, cDNA was prepared from 2µg of DNA-free RNA isolated from respective tissues. *TaARF* was used as an internal control for normalization of Ct values. Standard deviation was calculated along with its level of significance at $p<0.05$ (*) with respect to the first tissue. (D) Microarray based expression profiles of *TaVIH* genes.

Figure 2: Enzymatic activity and analysis of the substrate product on PAGE and MALDI-Tof MS analysis. (A) The relative luminescence units for all reactions performed were recorded using Spectramax optical reader. The kinase reactions were performed using 50 ng of VIH1 and VIH2 purified proteins. (B) The products were resolved in the 33% PAGE and stained with Toludene Blue using IP_6 (left panel) and IP_7 (right panel). Yeast VIP protein was used as a positive control. These experiments were repeated 3 times using and similar assays for product formation was obtained (C). MALDI-Tof MS analysis of synthesized products IP_7 and IP_8. MS analysis indicated a major signal at m/z of 739.009 that correspond to mass of IP_7 and IP_8 -adduct at 861.05 that matches with the expected generated species (details at supplementary Figure X).

Figure 3: Generation of VIH2-3B transgenic Arabidopsis and its characterization. (A) Western analysis and screening of Arabidopsis transgenic lines for VIH2-3B protein overexpressing lines. Multiple transgenic lines were screened and Western was done using His-Antibody using 20 ug of total protein. Coomassie Blue stain of the total protein (lower panel) was used as a loading control. (B) Representative picture of the rosettte area of the Transgenic Arabidopsis (#Line2, #Line4, #Line5 and #Line6) and controls. (C) Rosette area measurement (in cm2) using Image-J for 4 different transgenic lines along with the controls. Measurement was taken after 14 days of growth. (D) Number of Rosette leaves in transgenic Arabidopsis and control lines. Three experimental replicates using 10 plants each were used to calculate the parameters.

Figure 4: Morphological characterization of VIH2-3B transgenic Arabidopsis (A) Representative pictures of transgenic Arabidopsis and controls post 25 days of growth (flowering stage) and; length of main axis along with the leaves size (in mm). (B) Number of total shoots (primary and secondary shoots) in transgenic Arabidopsis and control plants (right panel). Left-panel show the morphological differences (as indicated by arrows) among the lines. For each transgenic line, three experimental replicates were performed using 10 plants each.

Figure 5: Drought response of VIH2-3B *Arabidopsis* transgenic lines. (A) Reporter assays using promTaVIH2:GUS transgenic lines subjected to drought-mimic (30% PEG). Seedlings

with or without treatment (control) were stained overnight in GUS staining solution and photographed using Leica stereomicroscope at 6.3X magnification. (B) Transgenic Arabidopsis and control seedlings were subjected to drought mimic conditions with glycerol-10 % and mannitol-125 mM. Ten seedlings were used for each transgenic line for each treatment. These experiments were repeated three experimental replicates with similar phenotype. (C) Root length of treated seedlings (in mm) for all the lines. Twenty seedlings were used for the measurement of root length for each line. (D) Relative water loss in Arabidopsis leaves post 12 hrs. Three experimental replicates each with ten leaves were used to calculate the water loss %. (E) Drought treatment of soil grown plants. Fifty-five seedlings pre-grown for the period of fourteen days were subjected to drought for additional fourteen days. The plants were then re-watered for the period of seven days and % survival rates were calculate. Representative pictures were taken post seven days of re-watering.

Figure 6: Interaction of TaVIH with TaFLA6 as identified during Y2H screening using TaVIH2-3B as a bait. (A) Y2H assay for the FLA6 and VIH interaction as represented by GAL plates containing -L-T and without GAL plates containing -HLT. (B) Pull down assay and Western analysis of the wheat FLA6 in the yeast strains. (C) Localization of FLA6 using HAtagged-TaFLA6 and TaVIH2 using cMYC tag. Fluorescence was measured using a Zeiss fluorescence microscope (Axio Imager Z2) with an Axiocam MRm camera at 63X. Representative images are shown and similar observations were noted for 3-4 independent transformed colonies of yeast. (D) Protein domain arrangement and hydrophobic plot for FLA6 domains with negative values represent hydrophilic regions.

Figure 7: RNAseq analysis of Col-0 and #Line4 and 6. (A) Expression pattern (as Z-scores) of top 56 genes commonly up-regulated among the transgenic lines w.r.t. Col-0(Ev) in 25 days old seedlings. Heatmap depicts the comparative expression in Col-0(Ev) and over-expressing lines of TaVIH2-3B (3 biological replicates; rep1-3). (B) Heatmap representing a graphical summary of the Gene Ontology (GO) classification for DEGs in #Line4 and #Line6 w.r.t. Control plants. Increasing intensities of brown and blue colors represent the comparative low and high expression for each gene, as depicted by the color scale. Normalized expression counts were used to plot the expression as Z-scores using heatmap.2 function from gplots package in R. Significantly altered GO terms were identified using Classification SuperViewer tool; x-axis represents the GO terms where bold terms represent significant alteration while y-axis represents the normed frequency which when > 1 signifies over-representation while <1 signifies under-representation.

Figure 8: RNAseq analysis of Col-0(Ev) overexpressing *TaVIH2-3B* Arabidopsis (#Line4 and 6). Heatmaps for expression patterns (as Z-scores) for genes DE in both transgenic lines w.r.t. Col-0(Ev), encoding for (A) Heatmap representing the comparative expression response of genes involved in cell wall related homeostasis that were DE in both the transgenic lines w.r.t Col-0(Ev). (B) ABA biosynthesis related pathway genes, (C) DREB encoding genes; (D) cytochrome P450 (CYPs) genes. Increasing intensities of brown and blue colors represent the comparative low and high expression for each gene, as depicted by the color scale. Normalized expression counts were used to plot the expression as Z-scores using heatmap.2 function from gplots package (Warnes et al., 2005) in R. Genes encoding for respective pathways were extracted using MapMan (Thimm et al., 2004). R1, R2 and R3 represent the biological replicates for the RNAseq analysis of the respective lines.

Figure 9: ABA and polysaccharides composition of Arabidopsis shoots and speculative model for the functioning of wheat VIH2. (A) ABA measurement in the leaves of transgenic Arabidopsis overexpressing VIH2-3B and control plants. (B) Venn diagram representation for the genes differentially regulated by drought stress, and transgenic lines #Line4 and #Line6 w.r.t. respective Controls. Drought responsive genes were shortlisted using the Cufflinks pipeline after processing the datasets for 10 days drought stress and control. (C) Mapman pathway analysis using Classification SuperViewer for the genes that are commonly regulated by drought stress (SRA: SRP075287) as well as transgenic lines w.r.t. control plants (#Line4 and 6). Bold terms represent significant pathways, normed frequency > 1 signifies over-representation while < 1 signifies under-representation. (D) For cell wall composition analysis wildtype Col-O, *Arabidopsis* overexpressing TaVIH2-3B (Line#2, 4, 5 and 6) and *Arabidopsis vih2-3* representing Arabidopsis mutant defective for the expression of AtVIH2 were used. Total AG: arabinogalactan, AX: arabinoxylan and Cellulose (in µg/g) was measured as indicated in Methods. Analyses were made in triplicates with each experimental replicate representing at least five plants for each genotype. Vertical bars represent the standard deviation. * on the bar indicates that the mean is significantly different at $p < 0.001$ (#at $p<0.05$) with respect to their respective control plants.

Figure 10: Speculative model for the working of VIH2 to impart drought resistance to plants. VIH2 could be involved in cell wall related developments via FLA like proteins or by causing changes in the stomatal distribution. Bothe the effects might contribute for the drought response in transgenic Arabidopsis.

Legends for Supplementary Figures and Tables

Supplementary Figure S1: Kyte-Doolittle Hydropathy plots and conserved domains of wheat VIH proteins. (A) Kyte-Doolittle hydropathy plots with the positive values indicating the hydrophobic domains and negative values represent hydrophilic regions of the amino acid residues. The hydropathy profile for proteins was calculated according to Kyte and Doolittle., 1982. (B) Schematic representation of domain architecture of TaVIH proteins deduced from CDD database: light gray rectangles indicate ATP Grasp/RimK Kinase domain and dark gray colored heaxgon correspond to Histidine Phosphatase superfamily.

Supplementary Figure S2: Expression patterns of *TaVIH* gene homoeologous in different tissues and stress conditions. RNAseq datasets of (A) Tissues and developmental stages (B) Abiotic (phosphate starvation, heat and drought stress) and (C) Biotic stress conditions were used. The expression values were obtained from expVIP database in the form of TPM values and ratios of stressed to control condition were used to generate heatmaps using MeV software. Green and red colors represent down-regulation and up-regulation of the genes in the specific stresses, as shown by the color bar.

Supplementary Figure S3: Three-dimensional (3D) structure for TaVIH proteins based on homology modelling and yeast complementation assays. (A) TaVIH2-3B overall structure depicting the AMP-PNP ligand accommodated by two anti-paralled beta-sheets. (B) hPPIP5K2, TaVIH1-4D, and TaVIH2-3B depicting the conserved catalytic residues in the IP6/IHP binding pocket. The key conserved residues are depicted using sticks and the green spheres represent Mg^{2+} ions. (C) Yeast complementation assay for *TaVIH* genes. Representative image of spotting assay performed on SD-Ura plates containing 1% raffinose, 2% galactose and supplemented with 0, 2.5 and 5mM of 6-azauracil. The wild type BY4741 and *vip1Δ* strains were transformed with respective constructs using Li-acetate method. Representative images were taken 4 days after spotting assay was performed. Similar results were obtained with three independent repeats. (D) Filamentous growth assays were observed for wild type yeast (WT), yeast mutant- *vip1Δ* with empty pYES2 (*vip1Δ*) and *TaVIH2-3B* complementation in vip1Δ- (*TaVIH2-3B*+ Δvip1). Pictures were taken 20 days post incubation.

Supplementary Figure S4: Purification and western analysis of purified wheat VIH1 and VIH2 kinase domain (KD) proteins. Both the VIH proteins (VIH1 and VIH2) were expressed and purified as mentioned in the Methods section and the expression was confirmed by the Western analysis using His-antibody.

Supplementary Figure S5: MALDI-ToF-MS analysis of the IP_7 from gel extracts. Gel purified inositol pyrophosphates from (A) IP_6 at 660.25 (B) VIH1 derived IP_7 at 739.8 and (C) VIH2 derived IP_7 at 739.00 were subjected to mass spectrometry analysis and m/z spectrum of IP_7 is shown. The peaks in the spectra describing as IP_6 and IP_7 are in agreement with the theoretical values for molecular weight that are deduced to be 660 and 740 Da.

Supplementary Figure S5: MALDI-ToF-MS analysis of the IP_7 and IP_8 from PAGE gel extracts. Gel purified inositol pyrophosphates from (A) IP_7 at m/z of 739.82 (generated by VIH1) (B) IP_7 at m/z of 739.009 (generated by VIH2); (C) IP_8 at m/z of 820.00 or its ACN adduct at m/z of 861.05 (generated by VIH1); (D) IP_8 adduct (CAN) at m/z of 861.05 (generated by VIH12). The peaks in the spectra describing as IP_7 and IP_8 are in agreement with the theoretical values for molecular weight.

Supplementary Figure S6: Hormonal and abiotic stress response of *TaVIH* genes promoter. (A) Cis-element analysis of VIH1 and VIH2 promoters (~1.5kb) Multiple stress related domains are represented in a schematic form. (B) Representative images for histochemical GUS assay performed against different stresses for promTaVIH1:GUS and promTaVIH2:GUS transgenic lines raised in *Arabidopsis thaliana* Col-0 background. Two week old seedlings selected positive against hygromycin selection on 0.5XMS agar plates were subjected to respective treatments: 1hr air drying for dehydration, heat stress at 37 ˚C for 8hrs, (-)Pi condition: 0.5XMS medias without KH_2PO_4 for 96 hrs, ABA (100µM), GA_3 (20µM) and NaCl (300mM) and drought (20% PEG) for 24hrs. Seedlings with or without treatment (control) were stained overnight in GUS staining solution and photographed using Leica stereomicroscope at 6.3X magnification.

Supplementary Figure S7: Western blot analysis, cDNA preparation and screening of the VIH interacting proteins (representative image). (A) Western analysis of c-MYC fused TaVIH1 or TaVIH2 proteins in the yeast strain. (B) Double strand cDNA preparation of wheat seedling library used for yeast two hybrid interaction studies. The cDNA library was resolved on the 1.2 % agarose gel. Two different cDNA preparations (Rep1 and Rep2) was performed and pooled together for the library preparation. (C) Representative yeast colony map for calculating the mating efficiency ($-LT_{1/1000}$). (D) Representative picture of the yeast colonies with putative interacting clones obtained on the selection plates (-AHLT+αGal). Each of the independent streaked colonies represent single putative interacting clone. Only colonies showing strong-blue coloration were used further for further study.

Supplementary Figure S8: Relative quantification of *TaVIH2* and its interacting partner during drought and development stages. (A) *TaVIH2* transcripts in Roots and Shoots of wheat

seedlings after 72 hrs of treatment with 5% PEG-8000 (CR-control roots; RT-root treatment; CS- control shoot; ST-shoot treatment. cDNA templates were prepared from 2 µg RNA isolated from samples of CR-Control root, RT-Root treatment with PEG, CS-Control shoot and ST-Shoot treatment. The Ct values were normalized against the reference gene *TaARF*. Respective standard deviation was calculated with their level of significance at $p<0.05$ (*) with respect to their respective control. (B Expression of *TaFLA6*, *TaGT* and *TaXat1 during different stages of development and* (C) during the drought condition for *(TaGT),* TraesCS6B02G339100 and *Xylan arabinosyl transferase (TaXat1),* TraesCS6A02G309400. Bar plot depicting fold change levels for *FLA6, TaGT* and *TaXat1* under drought condition post 1 and 6 hrs of stress.

Supplementary Figure S9: RNAseq analysis of transgenic Arabidopsis. (A) PCA analysis of the RNAseq for control (Col-0 (Ev)) and two transgenic Arabidopsis lines. (B) Map man analysis of the genes those are consistently represented in the two transgenic Arabidopsis lines with overexpressing TaVIH2-3B.

Supplementary Figure S10: Flow representation of the preparation and extraction of polysaccharides (Arabinogalactans, Arabinoxylans and Cellulose) form the shoots of *Arabidopsis*

Supplementary Figure S11: Standard graph for ABA measurement in plant leaves samples. (A) Y-axis indicates Log of concentration and X-axis indicates the optical density. Data was linearized by plotting the log of the target antigen concentrations versus the log of the OD and the best fit line was determined by regression analysis. (B) Panel showing the colour development for the quantitation of the ABA in different leaf samples, OD was taken at 420 nm.

Supplementary Table S1: List of *TaVIH* genes with computed physical and chemical parameters. The molecular weight and isoelectric point prediction were done using Expasy ProtParam tool (https://web.expasy.org/protparam/). The sub-cellular localization prediction was done using WoLF PSORT prediction tool (http://www.genscript.com/wolf-psort.html). RefSeq v1.1 for wheat Ensembl Plants was used for gene ID.

Supplementary Table S2: RPKM values of *TaVIH* genes' transcripts for normal (0 day) and phosphate starved (10 day) conditions in root and shoot tissues. The RNAseq data was used from Oono et al., 2014.

Supplementary Table S3: List of genes up- and down-regulated in #line4 (Sheets1,2) and line6 (Sheets3,4) w.r.t. Col-0(Ev) lines. DEGs were obtained using the Kallisto-DESeq2

pipeline; genes with LFC > 1 in either direction and padj < 0.05 were considered to be differentially regulated.

Supplementary Table S4: GC-MS analysis in shoot of *Arabidopsis* overexpressing *TaVIH2-3B*. Analysis was done for two independent extractions (independent extractions; Replicate1 and Replicate2; each using 4-5 pooled plants for respective lines). Inositol-derivative was used as an internal control as mentioned in the Methods section. Four independent transgenic lines (#Line2, 4, 5 and 6) along with control plants (Col-0 (Ev)) and mutant *vih2-3* line of Arabidopsis was used for analysis of Arabinogalactans (AG), Arabinoxylans (AX) and cellulose.

Supplementary Table S5: List of drought responsive genes that are differentially regulated in #line4 (Sheet1), #line6 (Sheet2), and differentially regulated in both #line4 and line6 (Sheet3). Drought responsive genes at 10days of drought stress w.r.t Control plants were extracted from the SRA RNAseq dataset (SRP075287) using Cufflinks pipeline. Genes with 1 > LFC < -1 were considered to be drought responsive.

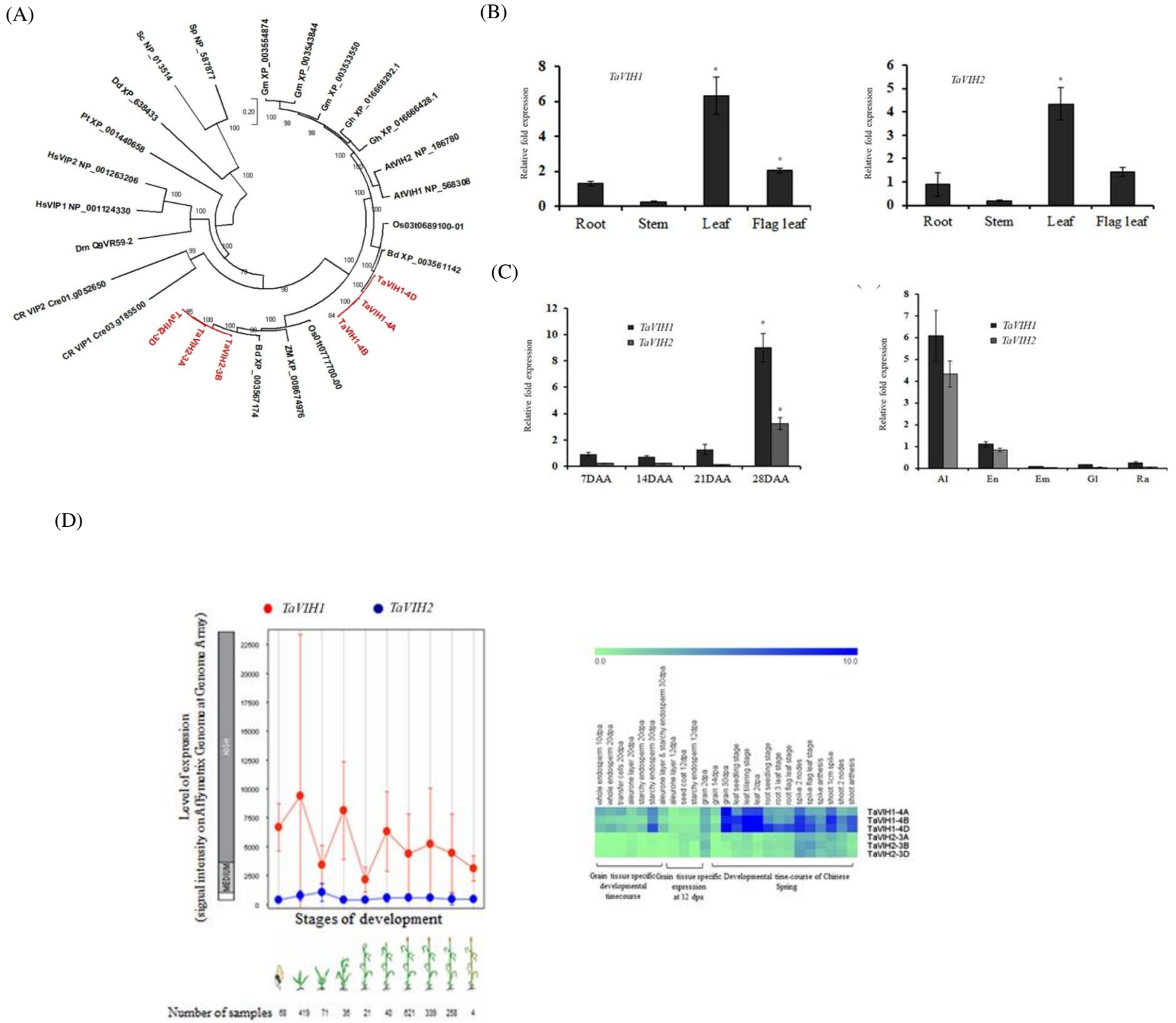

Figure 1

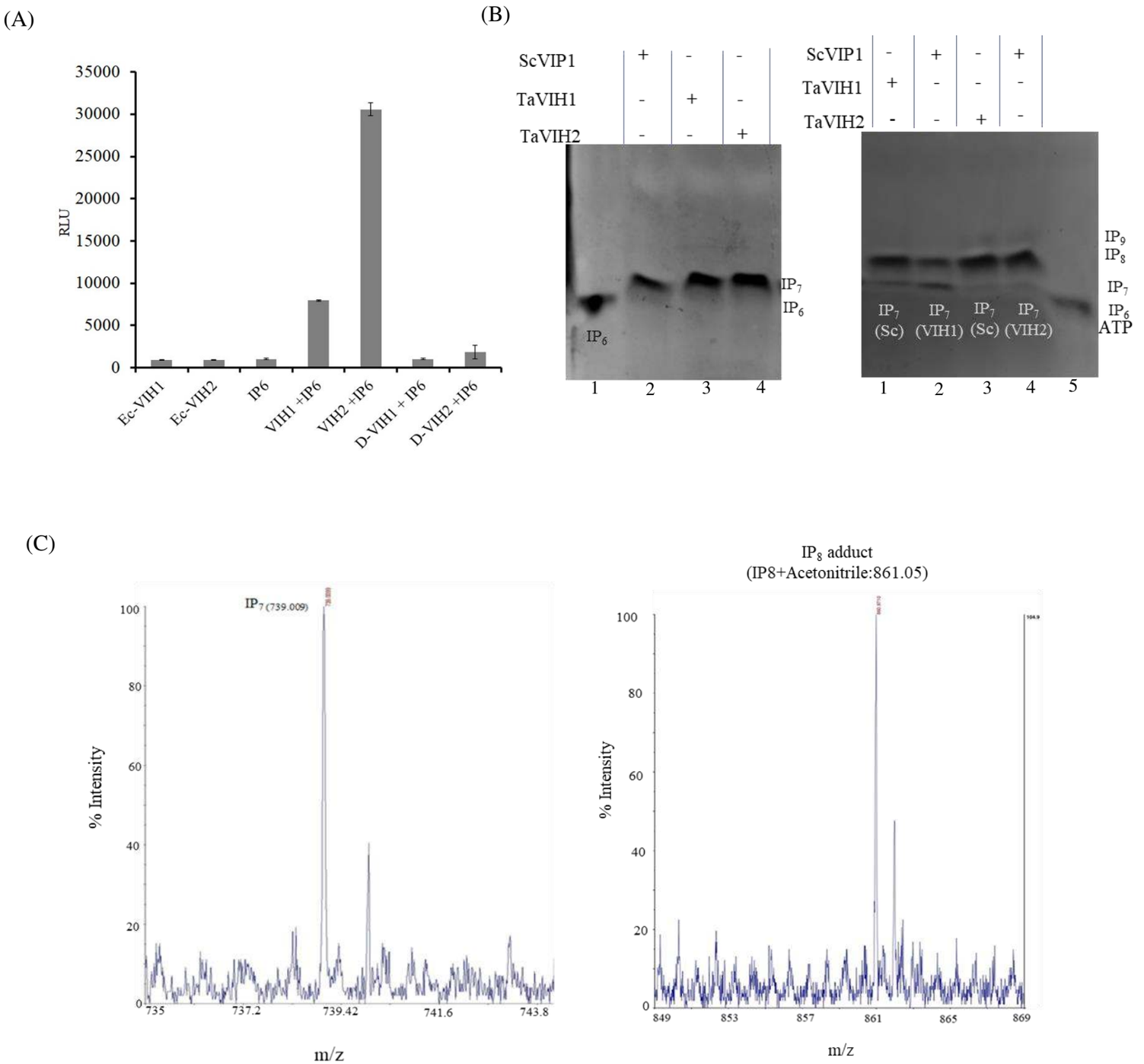

Figure 2

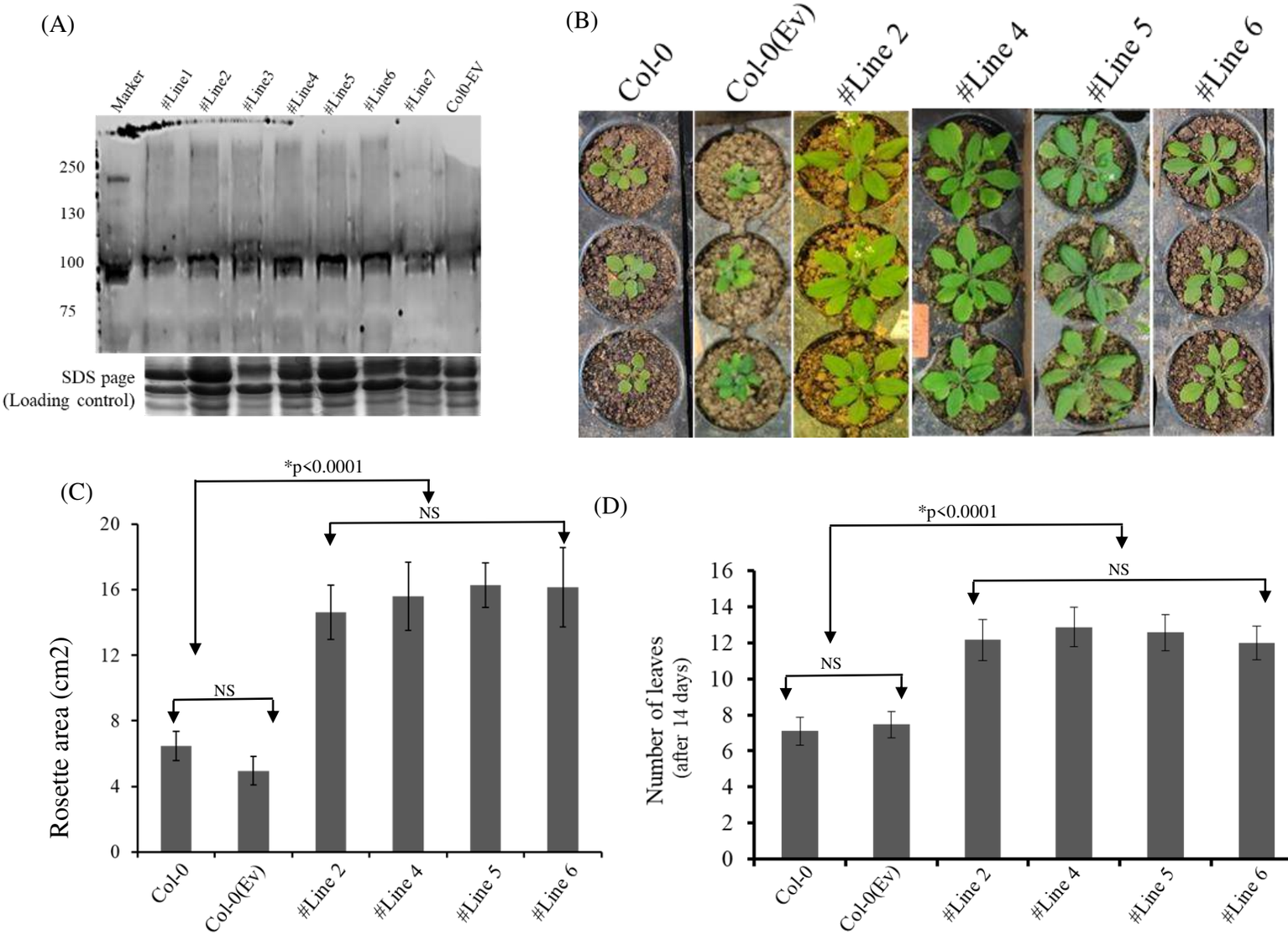

Figure 3

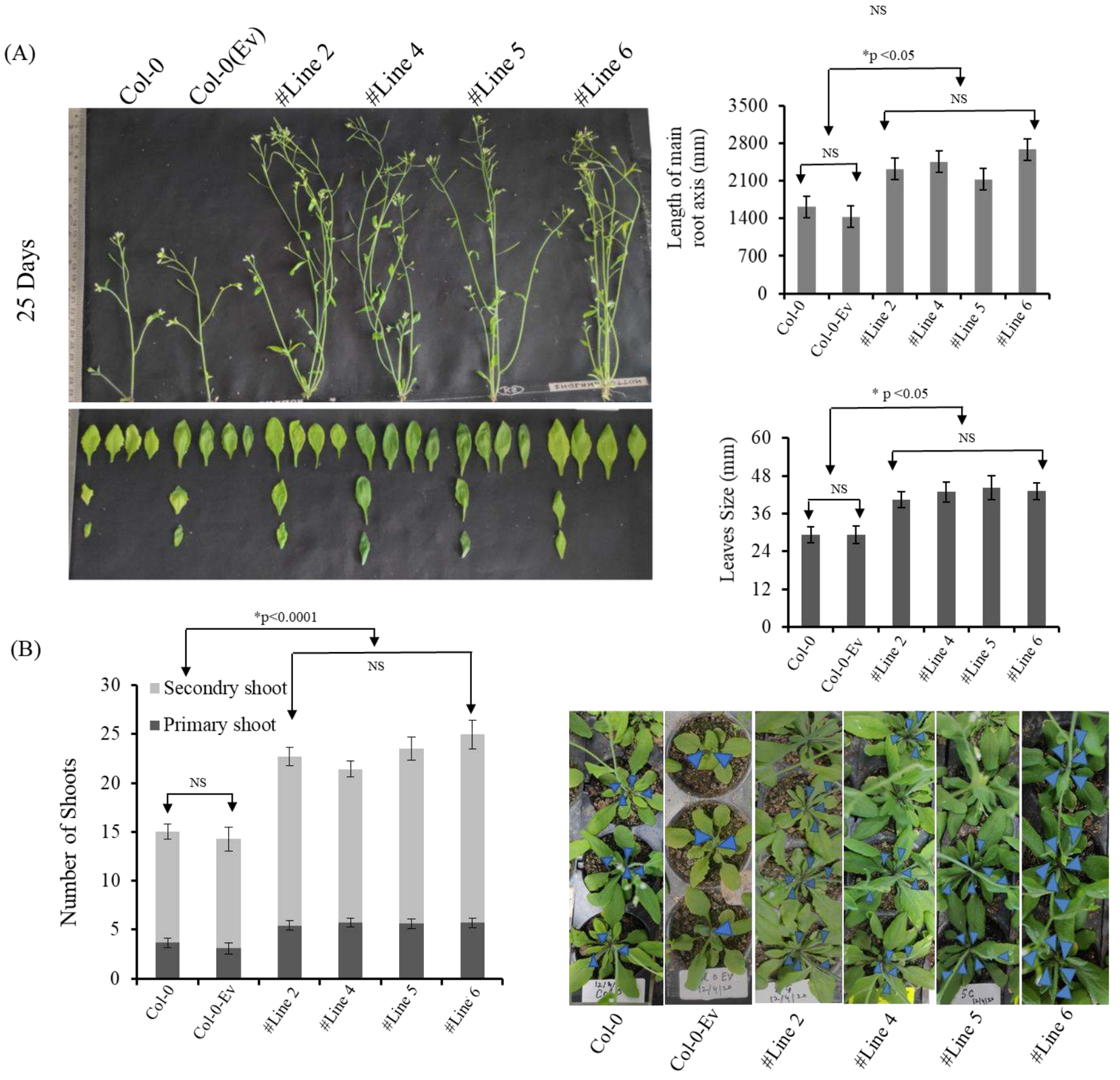

Figure 4

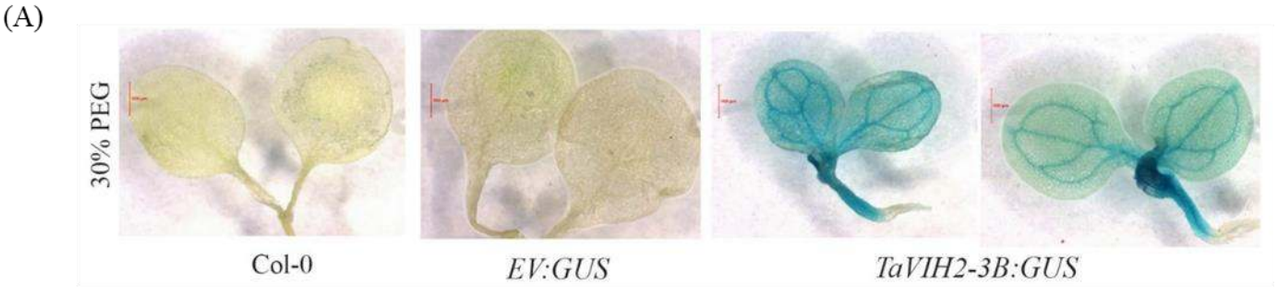

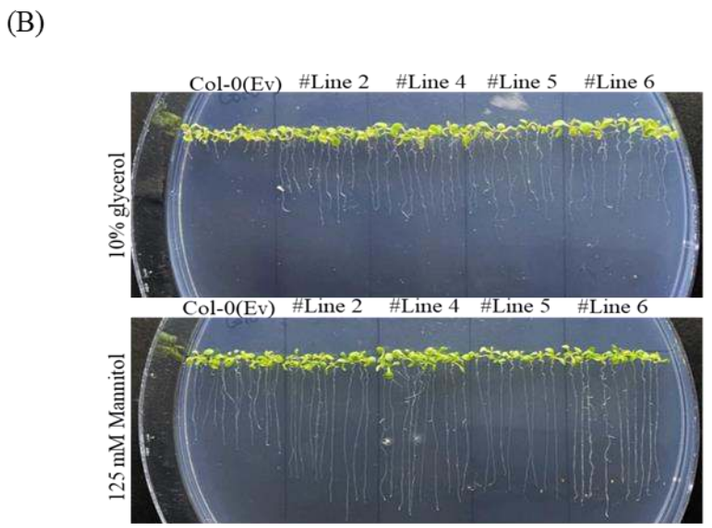

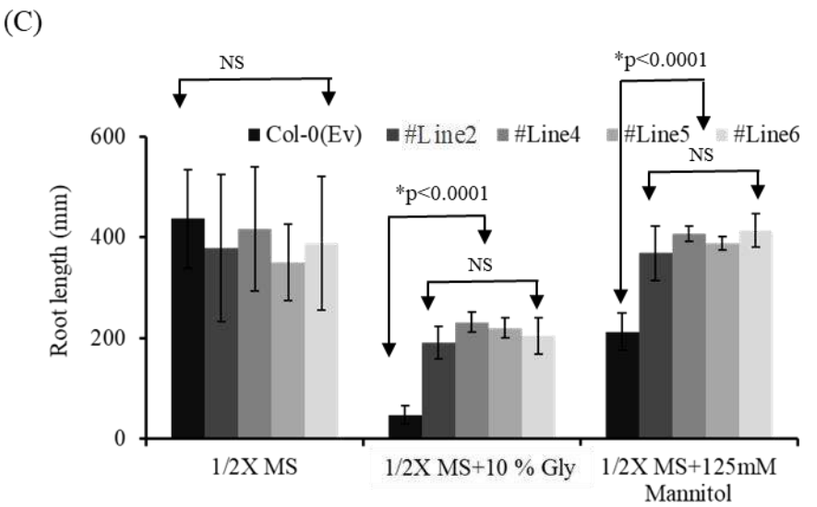

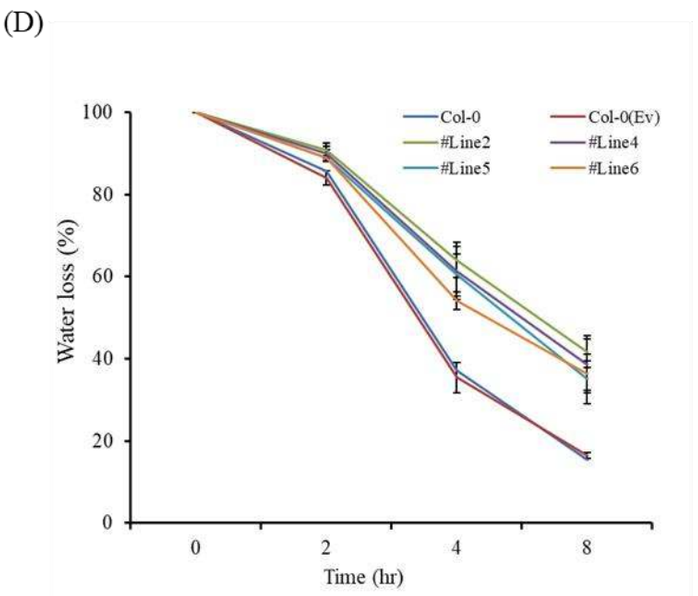

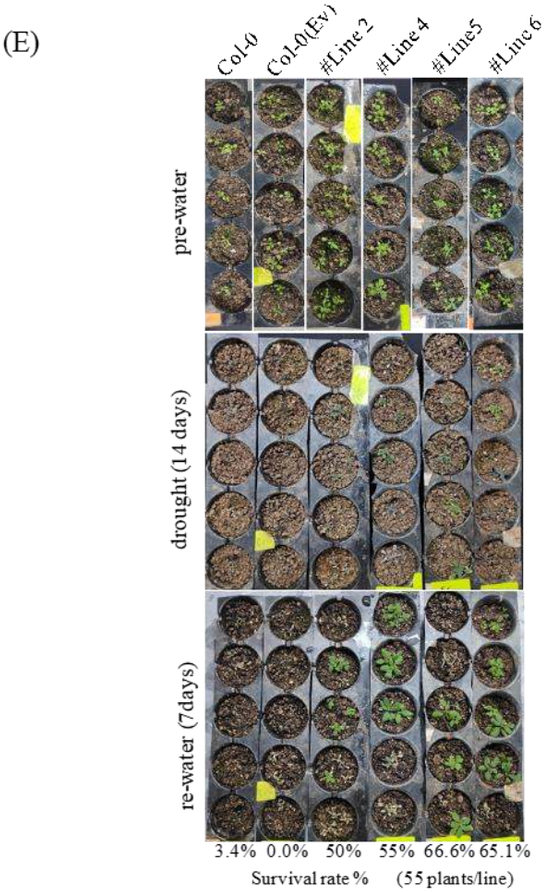

Figure 5

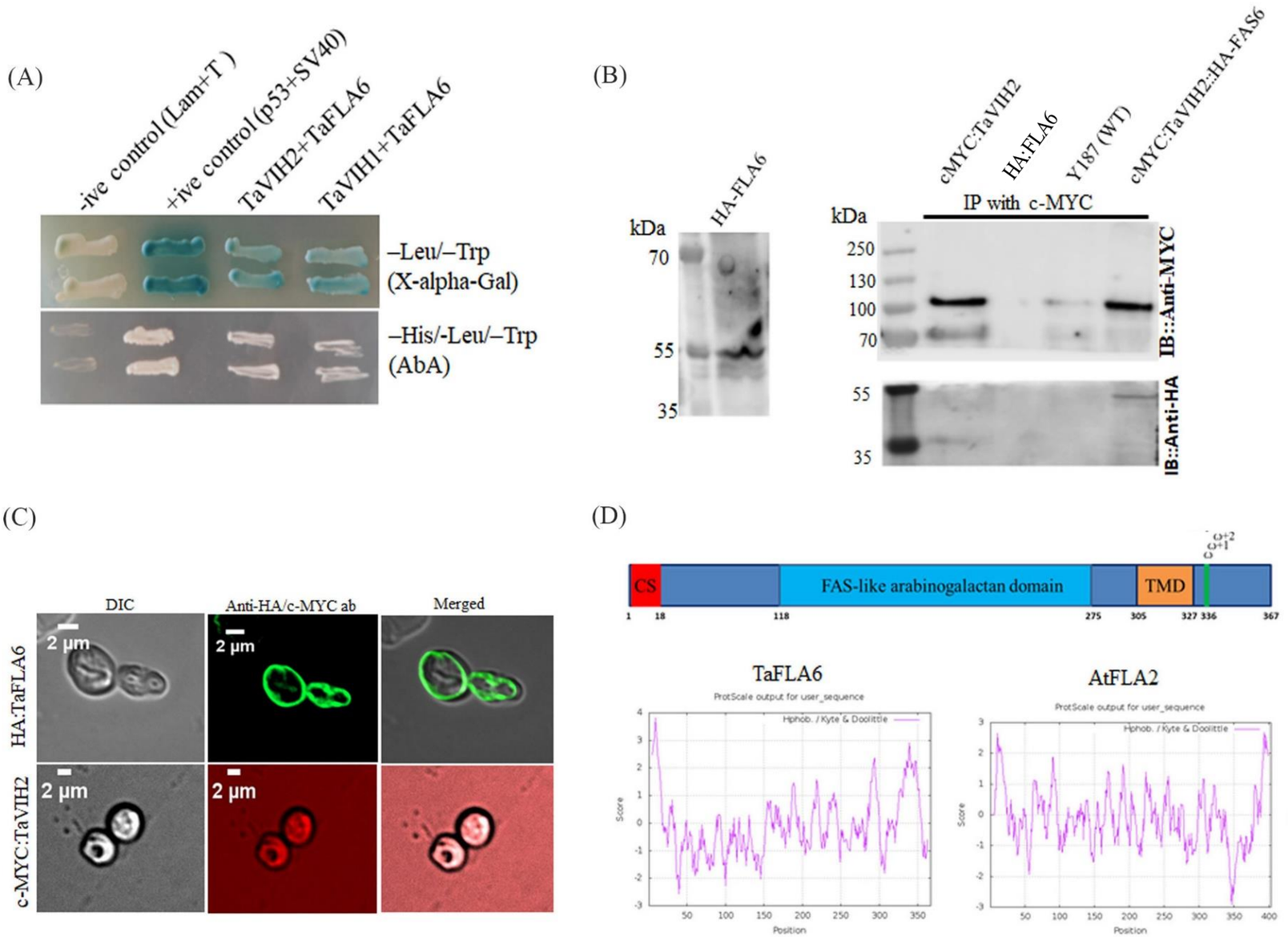

Figure 6

(A)

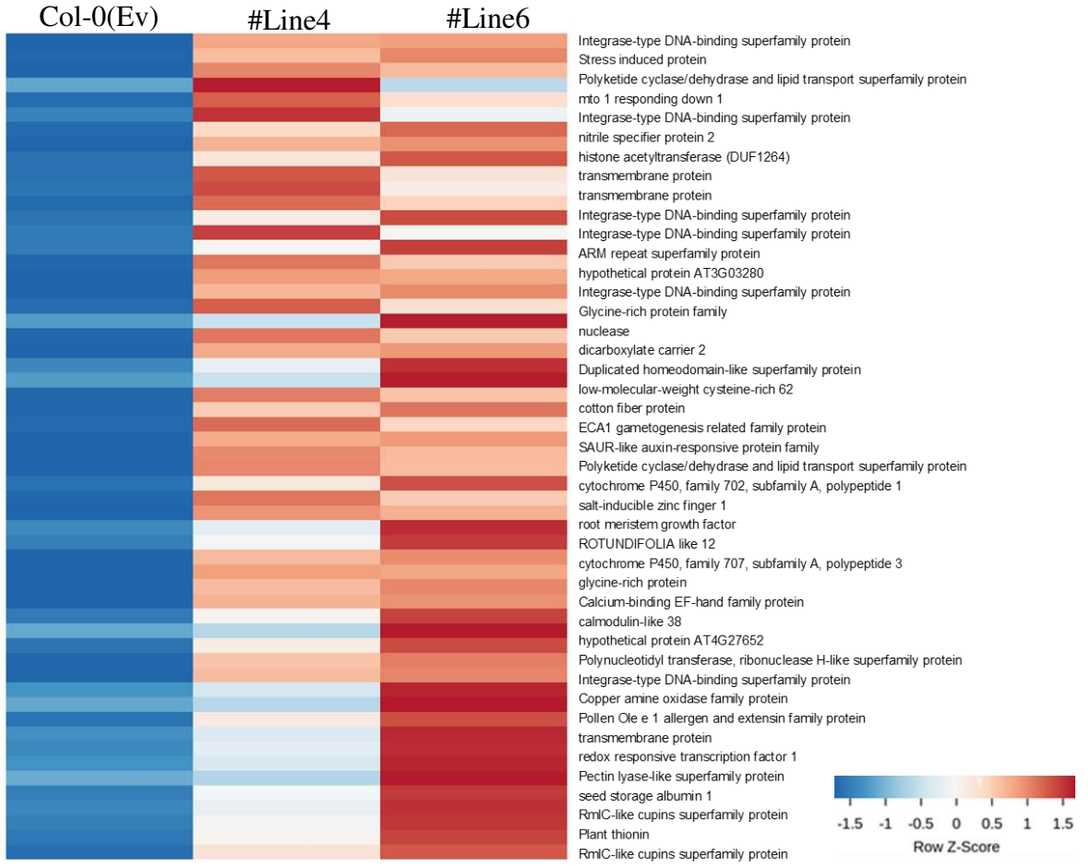

(B)

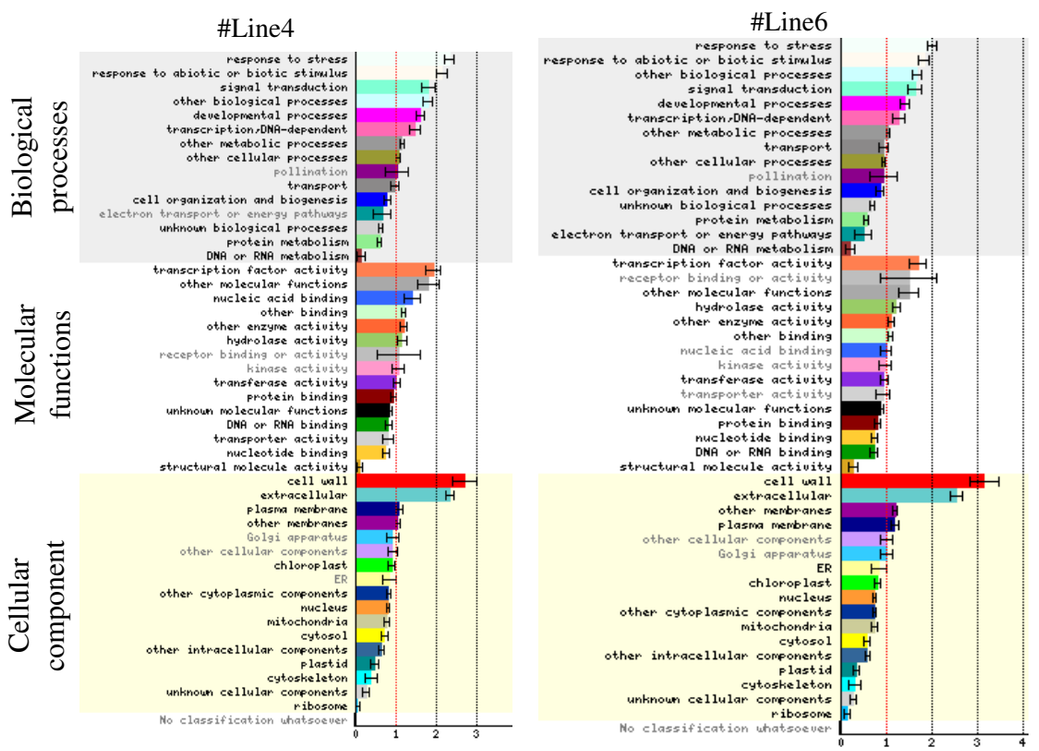

Figure 7

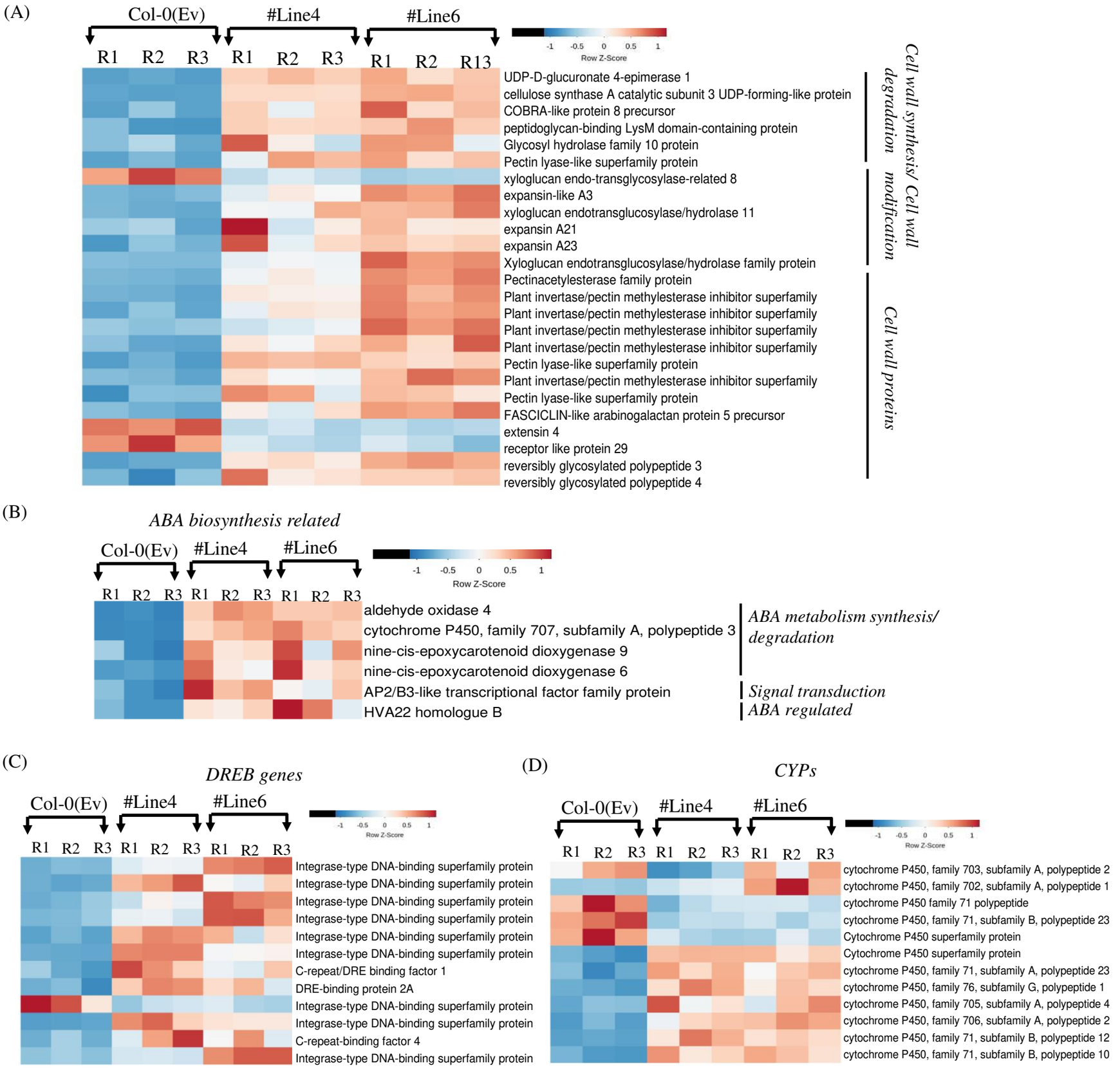

Figure 8

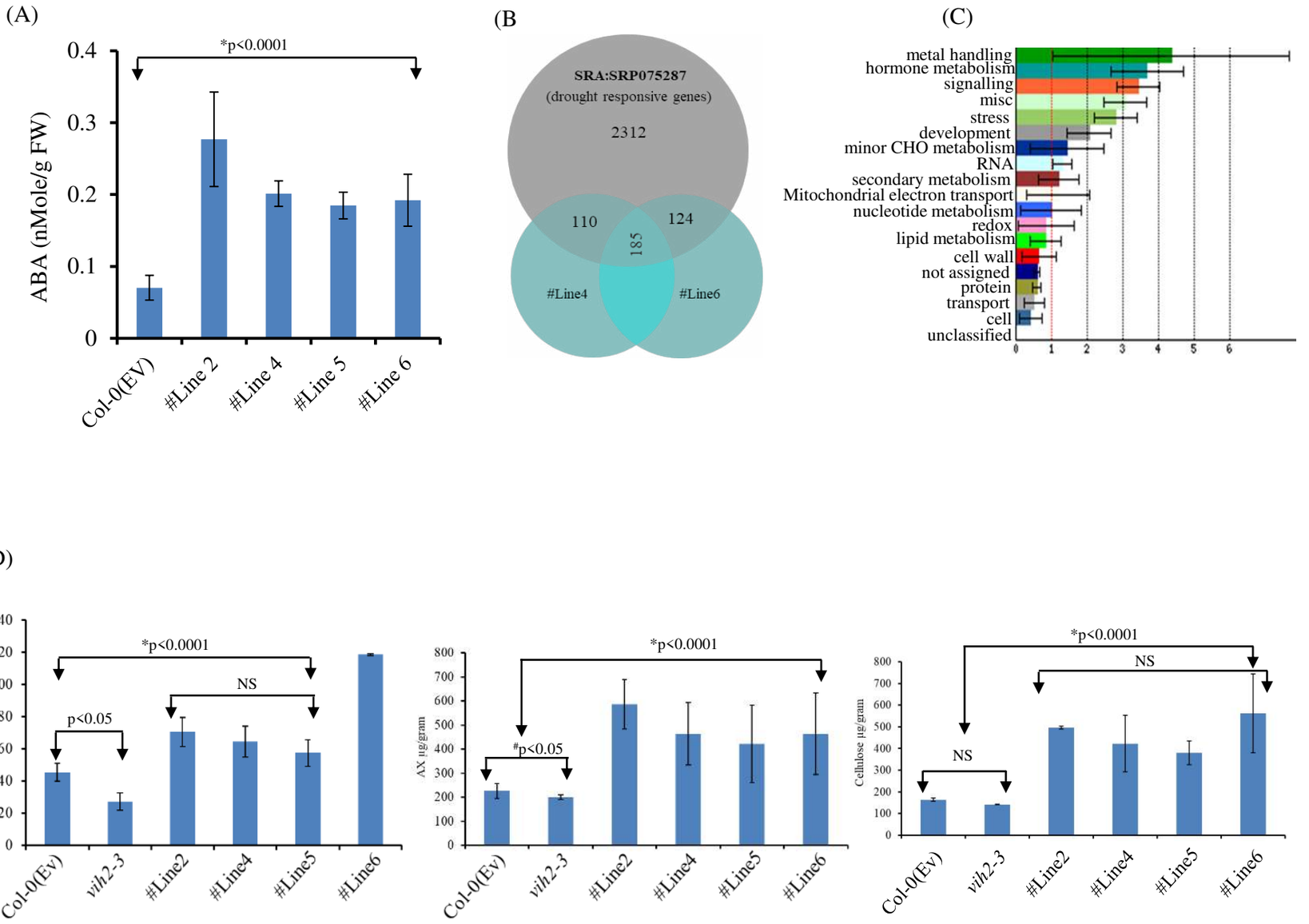

Figure 9

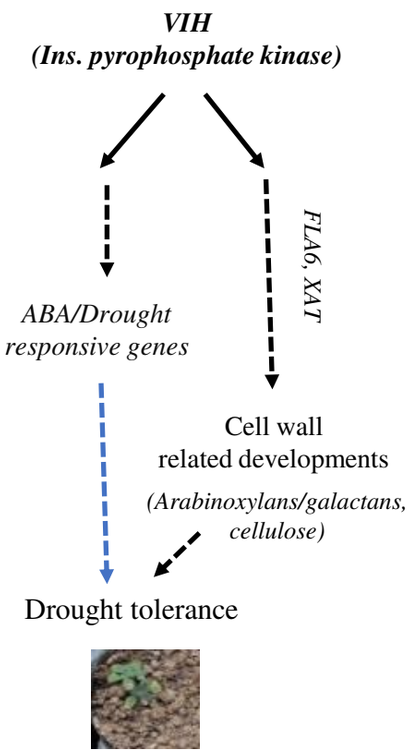

Figure 10